(12) INTERNATIONAL APPLICATION PUBLISHED UNDER THE PATENT COOPERATION TREATY (PCT)

(19) World Intellectual Property Organization
International Bureau

(43) International Publication Date
5 June 2008 (05.06.2008)

PCT

(10) International Publication Number
WO 2008/067528 A2

(51) International Patent Classification:
G01N 21/45 (2006.01)

(21) International Application Number:
PCT/US2007/086059

(22) International Filing Date:
30 November 2007 (30.11.2007)

(25) Filing Language: English

(26) Publication Language: English

(30) Priority Data:
60/867,961 30 November 2006 (30.11.2006) US
11/744,726 4 May 2007 (04.05.2007) US

(71) Applicant *(for all designated States except US)*: **PURDUE RESEARCH FOUNDATION** [US/US]; 3000 Kent Avenue, West Lafayette, IN 47906 (US).

(72) Inventors; and
(75) Inventors/Applicants *(for US only)*: **NOLTE, David, D.** [US/US]; 4155 Eisenhower Road, Lafayette, IN 47905 (US). **ZHAO, Ming** [CN/US]; 2601 Soldiers Home Road, Apt 36, West Lafayette, IN 47906 (US).

(74) Agent: **FILOMENA, Anthony, P**; Bose Mckinney & Evans LLP, 135 North Pennsylvania Street, Suite 2700, Indianapolis, IN 46204 (US).

(81) Designated States *(unless otherwise indicated, for every kind of national protection available)*: AE, AG, AL, AM, AT, AU, AZ, BA, BB, BG, BH, BR, BW, BY, BZ, CA, CH, CN, CO, CR, CU, CZ, DE, DK, DM, DO, DZ, EC, EE, EG, ES, FI, GB, GD, GE, GH, GM, GT, HN, HR, HU, ID, IL, IN, IS, JP, KE, KG, KM, KN, KP, KR, KZ, LA, LC, LK, LR, LS, LT, LU, LY, MA, MD, ME, MG, MK, MN, MW, MX, MY, MZ, NA, NG, NI, NO, NZ, OM, PG, PH, PL, PT, RO, RS, RU, SC, SD, SE, SG, SK, SL, SM, SV, SY, TJ, TM, TN, TR, TT, TZ, UA, UG, US, UZ, VC, VN, ZA, ZM, ZW.

(84) Designated States *(unless otherwise indicated, for every kind of regional protection available)*: ARIPO (BW, GH, GM, KE, LS, MW, MZ, NA, SD, SL, SZ, TZ, UG, ZM, ZW), Eurasian (AM, AZ, BY, KG, KZ, MD, RU, TJ, TM), European (AT, BE, BG, CH, CY, CZ, DE, DK, EE, ES, FI, FR, GB, GR, HU, IE, IS, IT, LT, LU, LV, MC, MT, NL, PL, PT, RO, SE, SI, SK, TR), OAPI (BF, BJ, CF, CG, CI, CM, GA, GN, GQ, GW, ML, MR, NE, SN, TD, TG).

Published:
— *without international search report and to be republished upon receipt of that report*

(54) **Title:** MOLECULAR INTERFEROMETRIC IMAGING PROCESS AND APPARATUS

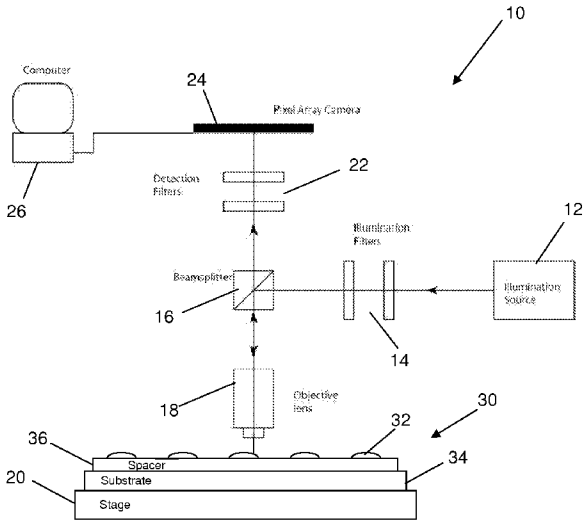

(57) **Abstract:** A molecular interferometric imaging system for detecting an analyte in a sample, that includes an illumination source providing a beam of radiation; a pixel array for detecting radiation in an image plane; a biolayer designed to react to the analyte when it comes in contact with the sample; a substrate designed to convert phase modulation into intensity modulation which can be detected and imaged directly by the pixel array, the biolayer being on the substrate; a reference surface; an image switching means for switching between a first position for collecting a sample image of the biolayer, and a second position for collecting a reference image of the reference surface; and a processing means for producing a composite image using the sample image and the reference image for illumination normalization.

WO 2008/067528 A2

MOLECULAR INTERFEROMETRIC IMAGING PROCESS AND APPARATUS

CROSS-REFERENCE TO RELATED APPLICATIONS

[0001] This application claims the benefit of U.S. Provisional Application Serial No. 60/867,961, filed on November 30, 2006, entitled "Molecular Interferometric Imaging Process and Apparatus," and U.S. Utility Application Serial No. 11/744,726, filed on May 4, 2007, entitled "Molecular Interferometric Imaging Process and Apparatus," which are both hereby incorporated herein by reference.

BACKGROUND AND SUMMARY

[0002] In the field of label-free biosensors, there is currently a large gap between the number of analytes that can be measured in a biological sample using existing systems, compared to the number of measurements required to understand the proteomic signature of health and disease. The measurement problem of proteomics is immense. A single cell can have as many as 10,000 expressed proteins, and each protein interacts with three or four others on average in cascaded networks of protein interactions. Optical biosensors have a potential advantage for this problem because of the intrinsic parallelism of light that allows multiple channels to be illuminated and detected simultaneously. Some imaging biosensors rely on this parallelism to some degree, but most do not tap the full resource that this parallelism represents.

[0003] In principle, it is possible to have over a million independent optical modes per square millimeter. There are two challenges to utilizing this billion-fold resource for optical biosensors. The first challenge is the preparation of the target that is to be interrogated. In the case of microarrays, the individual spatial modes need to be patterned with recognition molecules, e.g., antibodies, peptides or proteins. This represents a technological challenge that still has far to go. The second challenge, which is the readout of the billion optical modes, has already been partially met. High-end pixel arrays today have 10 million pixels, which is easily enough to measure the full mode density of an area 3 mm on a side. The other part of this challenge is the generation of a robust signal proportional to the amount of protein bound to the surface of the biosensor within a single pixel.

[0004] One of the more robust means of performing direct optical detection is common-path phase-quadrature interferometry, in which a signal carrying optical phase information from thin protein layers is combined with a reference wave that has a fixed relative phase of ninety degrees to produce an intensity shift proportional to the protein-

induced phase. The interferometry performs the function of a phase-to-intensity transducer. The common-path approach establishes and maintains quadrature independently of mechanical vibrations, making the system highly stable and low-noise.

[0005] The common-path interferometric approach to protein detection has been used with spinning-disc interferometry in the form of laser scanning on a biological compact disc. The biological compact disc can use single-mode illumination by a focused laser to scan bound protein on a spinning disc. There are several approaches to establishing and maintaining phase quadrature on a biological compact disc, including micro-diffraction, adaptive optics, phase contrast, and in-line. The advantages to high-speed sampling on a spinning platform include suppression of temporal 1/f noise, fast scan times, large-area microarrays, and high multiplexing. Conversely, the single-mode illumination used on a biological compact disc does not access the intrinsic parallel advantage of optical detection afforded by pixel arrays.

[0006] The present invention generally relates to obtaining direct images of biological molecules distributed on surfaces designed to convert molecular phase to reflected intensity. The reflected intensity is linearly proportional to protein density. Normally invisible biological molecules are made visible by the condition of in-line interferometric quadrature established by the substrate that transduces phase to intensity. The basic principle of operation is shearing in-line common-path interferometry in which a digital interferometric image of patterns of biological molecules is acquired and referenced to a reference surface by two image acquisitions. The technique has the advantage of high speed, high sensitivity and high-resolution optical detection of biological molecules.

[0007] The Quadraspec biological compact disc system described in U.S. Patent No. 6,685,885 acquires serial data on a single channel. However, it may also be advantageous in signal-to-noise (and hence sensitivity) applications to acquire many channels at the same time. With the present technique, a pixel array captures a plurality of pixel readings for each image. Moreover, while conventional laser scanning techniques are time-consuming when obtaining high-resolution scans of protein spots, as well as incompatible with disc wobble when scanning spots under high magnification, the present system minimizes these problems by acquiring numerous pixels in a single exposure. In addition, the focus of the microscope can be adjusted for each well, and even at a lower magnification, an entire "well" of spots can be seen in the field of view. As such, all the protein spots are acquired at the same time and under the same conditions.

[0008] Conventional laser scanning interferometric approaches are also incompatible with real-time kinetic captures from wet samples, particularly as flow-cell plumbing is impossible, except for the use of centrifugal force to move fluids. The present system can image through a flow-cell and system, thereby making it much more like surface plasmon resonance ("SPR") systems.

[0009] However, there are several advantages of the present system over SPR techniques, particularly as the present technology is easier to implement and has a higher sensitivity than SPR technology. The present system uses a non-resonant quadrature condition, thus the operating condition is relatively insensitive to spacer thickness or wavelength. SPR systems, on the other hand, are sensitive to thicknesses and require tightly constrained wavelengths and angles. The goal of quadrature detection is to suppress noise rather than to boost signal which frees it from operating-point drift and allows it to be multiplexed over large areas. The present system also has minimal restrictions on operating wavelength or angle. The quadrature conditions can be achieved at either surface-normal or higher angles. Operation at 30° is achievable without loss in sensitivity. The optimal wavelength is also defined within a relatively broad range of tens of nanometers.

[0010] Because the operation of the present system is so robust, the noise is very low, thereby giving higher signal-to-noise ratios than SPR approaches. It is anticipated that molecular interferometric imaging will have a surface mass sensitivity of one to two orders of magnitude better than SPR. In addition, the thickness of the spacer that establishes the quadrature condition does not have to be tightly constrained. A 20% drift in thickness across a platform causes almost no change in operating sensitivity. Moreover, the loose requirements on spacer thickness and operating wavelength allows a large area to be manufactured that does not have significant sensitivity drift across the platform. This allows large-area multiplexing.

[0011] The revolution in digital cameras over the past decade has provided increasingly more powerful CCD cameras at approximately level cost, making massively parallel channel acquisition accessible and commonplace in the laboratory and in the marketplace. The CCD cameras are participating increasingly in the field of biosensors, for instance being used in imaging ellipsometry and in surface plasmon resonance systems, as well as in the conventional arena of fluorescent array readers. The present invention introduces a new digital camera-based biosensor that is particularly easy to implement that detects protein on modified silicon surfaces with molecular sensitivity nearly down to the single-molecule limit.

[0012] The metrology limit of molecular interferometric imaging is 10 picometer/pixel longitudinal resolution at 0.4 micron diffraction-limited lateral resolution, corresponding to 1.7 attogram of protein. This is only about 8 antibody molecules per pixel, which is near to single-molecule detection. The scaling mass sensitivity of this technique is defined as the mass per square root of detection area. This scaling sensitivity is an intrinsic property of the detection system, and is not related to the area over which data are averaged. For instance, surface plasmon sensors typically quote values of 1 to 10 pg/mm$_2$ as their smallest detectable surface mass density. However, the area of their sensor is implicitly included in this value. In the case of molecular interferometric imaging, the intrinsic scaling at the metrology limit is 5 fg/mm. If an area of 1 mm is used to average data, this corresponds to 5 fg/mm$_2$, which is 20 to 200 times more sensitive than typical surface plasmon sensors. This molecular-scale mass sensivity is due to the shot-noise-limited performance of the CCD camera, combined with the non-resonant character of the in-line quadrature that makes it particularly low-noise and stable.

[0013] The metrology limit of molecular interferometric imaging is primarily of academic interest, while applications would require extensive handling of the discs, including wet chemistry. In the case of practical immunoassays on our specific surface chemistries, the scaling sensitivity increases to approximately 40 fg/mm for assays read in air, and 160 fg/mm for assays read in water. This last sensitivity is still better than for most surface plasmon resonance sensors. Using this sensitivity, we have performed an assay for prostate-specific antigen with a detection limit of 60 pg/ml per spot-pair in the presence of high background. With 10 thousand spot-pairs on a disc, this would provide a significant resource for high-throughput assays. Conversely, if all the spots on the disc were used for a single assay, the limit of detection would decrease to approximately 1 pg/ml, which is at the bottom of the range for proteins in signalling and regulatory pathways. Clearly, the simplicity of molecular interferometric imaging combined with its molecular sensitivity show promise for future applications in high-throughput proteomics.

[0014] Additional features and advantages of the invention will become apparent to those skilled in the art upon consideration of the following detailed description of illustrated embodiments.

BRIEF DESCRIPTION OF THE DRAWINGS

[0015] Aspects of the present invention are more particularly described below with reference to the following figures, which illustrate exemplary embodiments of the present invention:

[0016] Figure 1 is a graph of responsivity to protein at different oxide thicknesses on silicon as a function of wavelength;

[0017] Figure 2 is a graph of experimental data values and a simulated response for protein responsivity as a function of increasing numerical aperture for 7x, 20x and 40x magnifications;

[0018] Figure 3 is a simplified schematic drawing of an embodiment of a molecular interferometric imaging system viewing a sample;

[0019] Figure 4 is a top-view of a portion of a sample to be characterized by the interferometric imaging system;

[0020] Figure 5 is a schematic of a method for normalizing the background variation with a differential image;

[0021] Figure 6A shows a raw image of 100 micron diameter protein spots under 20x magnification before normalizing;

[0022] Figure 6B shows the result of shearing interferometry under 20x magnification for the data in Figure 6A;

[0023] Figure 7A is a prescan image of a protein spot;

[0024] Figure 7B is a postscan image of the protein spot in Figure 7A;

[0025] Figure 7C is a difference image of the protein spot in Figures 7A and 7B;

[0026] Figure 8A is a histogram of the protein spot in Figure 7;

[0027] Figure 8B is a histogram of the land adjacent to the protein spot in figure 7;

[0028] Figure 9A is a direct image under 40x magnification of a protein spot on 120 nm oxide thickness acquired with a 12-bit CCD camera;

[0029] Figure 9B is a differential composite image of the protein spot shown in Figure 4 after shift and acquisition in which the color is proportional to the protein height;

[0030] Figure 10 is an example of a uniformly printed 120 micron diameter protein spot with a height of 1-2 nm and the full range scale of the image being -2 nm to +2 nm;

[0031] Figure 11 is a composite of several differential composite images of many different protein spots, all approximately 100 microns in diameter, on many discs showing many different morphologies;

[0032] Figure 12 shows a pseudo-three dimensional image of surface morphology of a printed spot with a pronounced outer ring having a ring height of approximately 0.7 microns;

[0033] Figure 13 is a graph of the height repeatability (standard deviation) in picometers as a function of the number of averaged images at both 40x and 4x objective magnification;

[0034] Figure 14 shows a pixel to pixel fluctuation of approximately 100 molecules for 1024 averaged images;

[0035] Figure 15 is a graph of measurement noise as a function of the number of images averaged;

[0036] Figure 16 shows a differential composite image of a protein without water and under water, showing that the protein spot remains visible under water with approximately a factor of three reduction in signal intensity;

[0037] Figure 17 shows a simplified diagram of an arrangement for directly imaging a sample through a liquid using molecular interferometric imaging;

[0038] Figure 18 shows a simplified diagram of an arrangement for directly imaging a sample that is immersed in liquid using molecular interferometric imaging without imaging through the liquid;

[0039] Figure 19 is a graph of experimental data from real-time binding showing an increase in spot height for the specific spots, and a decrease in spot height for the non-specific reference spots versus image frames collected at 40 second intervals;

[0040] Figure 20A illustrates a multiple exposure image of a protein spot as it travels across the field of view;

[0041] Figure 20B illustrates a multiple exposure image of a uniform land as it travels across the field of view;

[0042] Figure 21A illustrates a time-lapse image of a protein spot as it travels across the field of view;

[0043] Figure 21B illustrates a time-lapse image of a uniform land as it travels across the field of view;

[0044] Figure 22 is a simplified schematic of an embodiment that requires no moving parts by using beam polarization to redirect the illuminating beam back and forth, depending on its vertical and horizontal polarization, either to a protein spot or to a reference surface

[0045] Figure 23 shows a color map of the results of a 128-multiplex assay (2 analytes per well over 64 wells) where the mouse concentrations were 0, 10, 100, and 1000

ng/ml (increasing downward on the vertical with BSA and rabbit concentrations varying along the horizontal), and the rabbit concentrations were 0, 1, 10 and 100 ng/ml (increasing on the horizontal with BSA and mouse concentrations varying along the vertical), and the final matrix is combined color (red = mouse, green = rabbit with equal mixture adding to yellow) and intensity (stronger for more bound mass);

[0046] Figure 24 shows histograms of pixel values for a single target-reference pair of spots for a PSA assay at 20x magnification where the incubation is at 10 ng/ml and the limit-of-detection (LOD) for a single pair is 60 pg/ml;

[0047] Figure 25 is an Interleukin-5 (IL-5) sandwich assay showing response as a function of antiben concentration where the limit of detection of the assay is 50 pg/ml;

[0048] Figure 26 shows a competitive assay in which the antigen competes against the protein A/G to bind the Fab secondary, the maximum binding to A/G at zero concentration minus the spot response is plotted versus increasing antigen concentration;

[0049] Figure 27A shows an antigen exposure study with secondary amplification with the kinetic curves showing the effect of increasing antigen incubation prior to the application of the secondary antibody;

[0050] Figure 27B shows the saturated relative height change as a function of antigen exposure; and

[0051] Figure 28 is a graph showing real-time binding in response to a series of protein exposures with a disc printed with protein G that binds the Fc region of IgG; the first step shows the binding of antibody to protein G, the second step is the binding of antigen, and the third step is the binding of the secondary sandwich antibody.

DETAILED DESCRIPTION OF EXEMPLARY EMBODIMENTS

[0052] The embodiments of the present invention described below are not intended to be exhaustive or to limit the invention to the precise forms disclosed in the following detailed description. Rather, the embodiments are chosen and described so that others skilled in the art may appreciate and understand the principles and practices of the present invention.

[0053] This application is related to U.S. Patent Application Serial No. 10/726,772, entitled "Adaptive Interferometric Multi-Analyte High-Speed Biosensor," filed December 3, 2003 (published on August 26, 2004 as U.S. Pat. Pub. No. 2004/0166593), which is a continuation-in-part of U.S. Patent No. 6,685,885, filed December 17, 2001 and issued February 3, 2004, the disclosures of which are all incorporated herein by this reference. This

application is also related to U.S. Patent Application Serial No. 11/345,462 entitled "Method and Apparatus for Phase Contrast Quadrature Interferometric Detection of an Immunoassay," filed February 1, 2006 (published on January 4, 2007 as U.S. Pat. Pub. No. 2007/0003436); and also U.S. Patent Application Serial No. 11/345,477 entitled "Multiplexed Biological Analyzer Planar Array Apparatus and Methods," filed February 1, 2006 (published on January 4, 2007 as U.S. Pat. Pub. No. 2007/0003925); and also U.S. Patent Application Serial No. 11/345,564, entitled "Laser Scanning Interferometric Surface Metrology," filed February 1, 2006 (published on November 16, 2006 as U.S. Pat. Pub. No. 2006/0256350); and also U.S. Patent Application Serial No. 11/345,566, entitled "Differentially Encoded Biological Analyzer Planar Array Apparatus and Methods," filed February 1, 2006 (published on February 1, 2007 as U.S. Pat. Pub. No. 2007/0023643), the disclosures of which are all incorporated herein by this reference.

[0054] Prior to describing various embodiments of the invention, the intended meaning of quadrature in the interferometric detection system(s) of the present invention is further explained. In some specific applications quadrature might be narrowly construed as what occurs in an interferometric system when a common optical "mode" is split into at least 2 "scattered" modes that differ in phase by about $N*\pi/2$ (N being an odd integer). However, as used in the present invention (and the previously referred to issued patents and/or pending applications of Nolte et al.) an interferometric system is in quadrature when at least one mode "interacts" with a target molecule and at least one of the other modes does not, where these modes differ in phase by about $N*\pi/2$ (N being an odd integer). This definition of quadrature is also applicable to interferometric systems in which the "other mode(s)," referring to other reference waves or beams, interact with a different molecule. The interferometric system may be considered to be substantially in the quadrature condition if the phase difference is $\pi/2$ (or $N*\pi/2$, wherein N is an odd integer) plus or minus approximately twenty or thirty percent. The phrase "in-phase" is intended to describe in-phase constructive interference, and "out of phase" is intended to describe substantially 180-degree-out-of-phase destructive interference. This is to distinguish these conditions, for both of which the field amplitudes add directly, from the condition of being "in phase quadrature" that describes a relative phase of an odd number of $\pi/2$.

[0055] Protein immobilized on a dielectric surface may be treated as an additional dielectric film that changes the reflection coefficient r of the surface. By fabricating a disc

with a proper reflected phase and amplitude, the reflectance change due to the protein can be maximized. For a protein layer of thickness *h*, the modified reflectivity is

$$r' = r + \left[\frac{(r_p - r)(1 - rr_p)}{(1 - r_p^{\,2})} + r \right] \frac{4\pi n_p}{\lambda} ih \qquad (1)$$

where r' is the protein-modified reflection coefficient, r_p is the reflection coefficient of the medium-protein interface, n_p is the refractive index of the protein layer, and λ is the wavelength of the probe light. This equation simplifies to

$$r' = r + i\pi \frac{(n_m^2 - n_p^2)(1+r)^2}{n_m \lambda} h = r(1 - iK \frac{1+r^2}{r} h) \qquad (2)$$

where n_m is the refractive index of the medium in which the dielectric surface is immersed. The medium can be air or water, where $K = -\pi \frac{n_m^2 - n_p^2}{n_m \lambda}$ is a real constant and h is the thickness of the protein layer.

[0056] Molecular interferometric imaging measures the protein density or the thickness of protein layer by monitoring the reflectance change $\Delta R = |r'|^2 - |r|^2$. The optical setup adopts in-line (IL) common-path interferometry in which the relative phases of the partial reflection from the protein and from the underlying substrate are nearly ninety degrees. The inline signal is described by

$$\begin{aligned} IL &= \left(\left| 1 - ik \frac{(1+r)^2}{r} h \right|^2 - 1 \right) |r|^2 \\ &= 2kh \, \mathrm{Im}\left(\frac{(1+r)^2}{r} \right) |r|^2 \qquad (3) \\ &= 2kh \, \mathrm{Im}(r + \frac{1}{r}) |r|^2 \end{aligned}$$

This equation reaches a maximum when $r = \pm i/\sqrt{3}$. The sensitivity of protein detection would be maximized at this working condition, called the quadrature condition for in-line detection. In practice it is not necessary to fabricate a disc to have exactly this reflectivity.

[0057] A simple substrate with which to work is a thermal silicon oxide on silicon. For a two-layer system like this, the reflection coefficient r is given by

$$r = \frac{r_1 + r_2 e^{-2i\delta}}{1 + r_1 r_2 e^{-2i\delta}} \tag{4}$$

where r_1 is the reflection coefficient of the air-oxide interface, and r_2 is the reflection coefficient of the oxide-silicon interface. The optical phase shift δ of the incident light that travels through the oxide layer is given by

$$\delta = \frac{2\pi n_1 h \cos\phi_1}{\lambda} \tag{5}$$

where n_1 is the refractive index of the silicon dioxide, h is the thickness of the oxide layer, and ϕ_1 is the angle of the incident light in the oxide layer. Figure 1 shows the dependence of the system response as a function of wavelength and oxide thickness. For our experiment, we use 630 nm wavelength, and an oxide thickness of 120 nm. The protein response for this condition is calculated by Eq. (3) to be 1.6%/nm for a protein layer with a refractive index of 1.4.

[0058] The theoretical responsivity is based on normal-incident light. However, when a microscope objective is used, the numerical aperture (NA) of the objective requires oblique-incident light to be considered. For oblique-incident light with an incident angle of ϕ_0, the response of the inline quadrature interference is approximately

$$IL = 2kh\,\mathrm{Im}(r(\phi_0) + \frac{1}{r(\phi_0)})\left|r(\phi_0)\right|^2 \cos\phi_0 \tag{6}$$

in which $r(\phi_0)$ is also a function of the incident angle. When a microscope objective with a large NA is used, the resulting response is integrated over the collection angle because of the

large angular bandwidth, which reduces the system responsivity. Figure 2 shows the system response as a function of numerical aperture for a uniform distribution of incident light intensity. The data in the figure are the measured protein response using objectives with NA of 0.12 (7x), 0.45 (20x) and 0.65 (40x). The simulated system response agrees reasonably well with the experimental measurements.

[0059] Figure 3 shows a basic schematic of an embodiment 10 of a molecular interferometric imaging system viewing a sample 30. The sample 30 is placed on a stage 20 of the system 10. The sample 30 is not shown to scale in Figure 3 to ease viewing and description. The sample 30 includes a biolayer 32 that is located on a substrate 34. In some embodiments a spacer 36 is located between the biolayer 32 and the substrate 36. Figure 4 shows a top-view of a portion of the sample 30 to be characterized by the system 10. The sample 30 includes the biolayer 32 that is to be analyzed by the system 10 and a land 33 that acts as a reference surface. When there is a spacer 36, the spacer 36 can act as the land 33; and when the biolayer 32 is applied directly to the substrate 34, the substrate 34 can act as the land 33. As an example, one embodiment of the sample 30 can include silicon as the substrate 34 with an oxide layer as the spacer 36, and the oxide thickness selected to put the system in an in-line quadrature condition (typically 120 nm). In this embodiment, the biolayer 32 can include a plurality of spots containing a capture antibody deposited on the spacer 36, and when a specimen containing the analyte is applied to the sample 30, the analyte is captured by the antibody in the biolayer 32.

[0060] A radiation beam from an illumination source 12 passes through illumination filters 14 and into a beam splitter 16 which directs the incident beam through an objective lens 18 onto the sample 30. The reflected beam from the sample 30 passes back through the objective lens 18 and the beam splitter 16. The reflected beam then passes through detection filters 22 and onto a pixel array camera 24. The pixel array camera 24 is connected to a computer 26 which stores the reflected image of the sample 30. If the light source 12 is a laser tuned to the appropriate quadrature condition for the spacer 36 of the sample 30, then either or both of the filters 14 and 22 are optional. However, if the light source 12 is a broad-band source (such as an incandescent light or a halogen lamp) then at least the illumination filters 14 would be necessary.

[0061] An experimental embodiment of the system shown in Figure 3 was designed with monochromic light from the light source 12 directed into a reflective microscope (Leica DMR) and focused onto the sample 30 by the microscope objective 18. The reflected light is collected by the same objective 18 and imaged onto the camera 24 that captures the images to

the computer 26. Two light sources have been used in the experiment. One is a 10 mW LED with a center wavelength at 630 nm and a 30 nm bandwidth (eLED). The top of the LED is flattened to obtain more uniform illumination. The other light source is an Oriel model 66187 halogen lamp with 10 nm band-pass filters at wavelengths 635 nm, 532 nm and 440 nm. Thus far, the LED has been found to be more stable than the halogen lamp, with smaller intensity fluctuations over time.

[0062] In the experimental embodiment the microscope has several objective lenses 18. The light from the light source 12 is directed into the microscope and focused onto the sample 30 by microscope objectives 18 with 7x, 20x or 40x magnification. The 7x objective is a 4x Nikon 0.17 m corrected objective, which when coupled with the infinity-corrected Leica microscope, produces an effective magnification of 7x. The corresponding pixel resolutions are 2.2 μm, 0.72 μm and 0.36 μm, respectively, which are calibrated by a test chart with 100 μm size features.

[0063] In the experimental embodiment, the camera 24 is a 12-bit QImaging 4000R interline CCD camera, with 2048x2048 7.4 μm pixels. Because of the interline format of the pixel array, the effective size of each pixel is 14.8 μm. At 40x magnification, this corresponds to a 0.37 μm surface area on the sample. The Arie diffraction limit at 630 nm wavelength is 0.39 μm, which is about the same as the pixel resolution at 40x. The full-well depth of the CCD is 40,000 electrons, with a read-out noise of 10 electrons. The measured photon transfer curve of the CCD camera showed that the noise of the CCD pixels starts at 10 electrons, and increases as the square-root of the number of electrons per well up to nearly the full well. This demonstrates that the noise of the CCD is dominated by photon shot-noise when operated close to full well. Therefore, we typically operate the CCD at 30,000 electron per well per acquisition, to acquire as many photons as possible while staying away from non-linearity near full well.

[0064] A differential composite image is obtained by acquiring an image of the biolayer 32 and an image of the land 33, and then differencing the two images. The adjacent land acts as the reference surface for illumination normalization.

[0065] The substrate 34 and spacer 36 are configured to convert phase modulation to reflected intensity so that it can be detected and imaged directly by the pixel array 24. This phase-to-intensity conversion takes place through in-line quadrature interferometry which is described in U.S. Patent Application Serial No. 11/675,359, entitled "In-Line Quadrature and Anti-Reflection Enhanced Phase Quadrature Interferometric Detection," which was filed on

February 15, 2007, and in International Application Number PCT/US07/62229, entitled "In-Line Quadrature and Anti-Reflection Enhanced Phase Quadrature Interferometric Detection," which was also filed on February 15, 2007, both of which are hereby incorporated herein by reference. The light reflected from the biological molecules has a quadrature condition relative to light reflected from an in-line reference surface. This converts the phase modulation caused by the light interacting with the molecular dipoles to interfere in the far-field with the reference light to create the intensity modulation that is proportional to the phase modulation. The equation describing this process is:

$$\Delta I = 2\sqrt{I_{ref}\, I_{signal}}\ \Delta\phi \tag{7}$$

where the phase modulation caused by the molecules is:

$$\Delta\phi = \frac{4\pi}{\lambda}\left(n_b - n_m\right)d \tag{8}$$

where d is the effective thickness of the biolayer, n_b is the refractive index of the biolayer, and n_m is the refractive index of the surrounding medium. From a molecular point of view there is not a biolayer but rather a scattered distribution of molecules on the surface. Then the modulated phase is:

$$\Delta\phi = \frac{4\pi}{\lambda}\left(n_b - n_m\right)\frac{2\pi r_m^3}{3r_s^2} \tag{9}$$

where r_m is the molecular radius of gyration, and r_s is the average molecular separation on the surface. The refractive index in this case is the refractive index associated with the individual molecules.

[0066] In the experiments, the substrates used were 100 mm diameter silicon wafers coated with 120 nm of thermal oxide. The top SiO_2 surface was functionalized to bind protein covalently. Two surface chemistries were used for the immobilization of protein onto the surface. One was based on di-isocynate, and the other based on butyraldehyde. For the di-isocyanate coating, the discs were first plasma cleaned, followed by a deposition of a hydrophobic barrier that separates the disc into 84 or 96 wells. The surface is functionalized by vapor phase deposition of aminopropaldimethyl ethoxy silane (APDMES) that covalently binds protein through a di-isocyanate crosslinker. For the butyraldehyde discs, the discs were cleaned by an SC-1 process that involves heating the discs in a 10:1:1 dilute solution of DI water, 30% hydrogen peroxide and 30% ammonium hydroxide. The disc surface was silanized in gas-phase deposition of triethoxysilylbutylaldehyde, after which the hydrophobic barrier was deposited onto the surface.

[0067] Protein spots were printed in 300 pL spots by a Piezo ink-jet printer (Scienion Inc.). Proteins solutions are prepared in PBS buffer. The resulting diameter of the spots is about 150 microns. After the print, the spots were incubated in 75% humidity condition for 1 hour to immobilize on the di-isocynate coating. The disc was then washed with PBS buffer containing 0.05% Tween 20 followed by DI water. The remaining functional surface was blocked by ethanolamine, and the discs were passivated in a 0.05% casein solution with 0.05% Tween 20.

[0068] The intensity modulation ΔI caused by the biolayer 32 is often small, in the range of a few percent of the total reflected light intensity. When measured directly, it is dominated by the spatial inhomogeneity of the illumination, which is the spatial 1/f noise of the system and can be much larger than the protein-induced intensity modulation. To remove the spatial 1/f noise, shearing interferometry can be performed using the land 33 to normalize this background variation and make the protein structures clear. The land 33 has substantially no protein on it and acts as a normalization surface.

[0069] Figure 5 shows schematically an example of shearing interferometry. In this example, a portion of a biological compact disc 40 is shown that has a protein spot 44, a lower adjacent land 43, and an upper adjacent land 45. A first image 41 is taken of the protein spot 44 using the imaging system 10 which includes the lower adjacent land 43. The disc 40 is then shifted in the field of view of the system 10 and a second image 42 is taken of the protein spot 44 using the imaging system 10 which includes the upper adjacent land 45. The spatial profile of the illumination remains unchanged during the shift, and can be normalized out. The normalization procedure uses the two images 41 and 42. A composite differential image 47 is computed on a pixel-by-pixel basis as:

$$I_{Diff} = 2\frac{(I_A - I_B)}{(I_A + I_B)} \qquad (10)$$

where I_A is a pixel value from the second image 42 and where I_B is the corresponding pixel value from the first image 41. The composite differential image 47 includes two versions of the protein spot 44: a negative difference version 46 (the land 45 of image 42 minus the protein spot 44 of image 41) and a positive difference version 48 (the protein spot 44 of image 42 minus the land 43 of image 41). The spot information in the image pair 46, 48 is the same, but the background is different. The difference compensates for the spatial variations in the illumination, and can be used to produce an image of the protein spot 44. It is preferable to use a combination of the image pair 46, 48 in subsequent data analysis to

provide for an average of the protein spot 44, but either 46 or 48 can be used alone. The magnitude of the spot height in the difference images 46, 48 are proportional to the amount of protein present in the spot 44.

[0070] Figure 6A shows the raw data acquired by the CCD camera. The protein spots are buried in the large background variation and almost invisible. Figure 6B shows the result of shearing interferometry for the data in Figure 6A. The spatial 1/f noise is removed, and the protein spot can by precisely measured. The result contains a positive image of the protein spot and a negative mirror image of the same spot. In this process, the protein spot is referenced against its adjacent land. Therefore the result of the shearing interferometry is surface height profile differenced to the adjacent land.

[0071] The land adjacent to a biological spot should be flat and clean to provide a good normalization surface. The land on both sides of a spot can be used for a single shift in one direction, but multiple shifts could also be used to try to balance directional systematics on the disc or wafer. For a single difference image of a spot and adjacent land, no registration is needed since the land is generally homogeneous. However, when taking many difference images and averaging them, then registration of the multiple difference images is preferred. Algorithms and software packages are commercially available to register images in microscopy. The normalization surface is not an interferometric reference surface. The interferometric reference surface is in-line, not lateral. The normalization surface takes effect after the reference-surface has already converted phase to intensity. The normalization removes spatial variations in the illumination.

[0072] In an immunoassay, the binding of protein is analyzed by differencing the height profile of the immobilized capture agent before and after incubation with a sample containing multiple analytes. An example is given in Figure 7 where the spot was anti-IL5 antibody with bound IL-5 that is binding secondary anti-IL5 from solution at a concentration of 100 ng/ml. The captured analyte exhibits a surface height increase of 0.12 nm. The protein spot was scanned with a 20x objective before (Figure 7A) and after incubation (Figure 7B). The two scan images of the same spot are then registered by cross-correlation and differenced. The difference image is shown in Figure 7C.

[0073] Figure 8A shows the histograms of the pre-scan spot, the post-scan spot and the difference. Both the spot print height in the prescan image and the binding of protein in the difference image follow closely to a Gaussian. Figure 8B shows histograms of an area of the same size as the spot on the land for the pre-scan, post-scan and difference, which shows

that the land is non-reactive and very flat, with surface height standard deviations less than 0.3 nm/pixel.

[0074] The following description provides greater detail on the eight basic elements of the embodiment of the in-line molecular interferometric imaging system 10 shown in Figure 3. There are many possible alternative embodiments for each of these elements.

[0075] The illumination source 12 could be any one of numerous illumination sources known in the art (e.g., incandescent; halogen; LED). The light source 12 can be coherent or incoherent, and single color or multiple color. High photon flux is provided by an LED or a superluminescent diode, but a more basic embodiment would be a white light source that is filtered.

[0076] The illumination filters 14 can be any one of numerous illumination filters known in the art (e.g., color; polarization; Fourier and image masks). Illumination filters can convert white light into single color or multiple color light. Multiple colors could be selected to coincide with the two opposite in-line quadrature conditions set by the substrate. By matching the detection filters 22 to the illumination filters 14 differential color composite images can be composed to isolate protein relative to scattered light or absorbed light. If the filters are in the UV, then protein or DNA spectroscopy becomes possible because of the optical transitions in the UV. The combination of in-phase with quadrature information in interferometry provides a complete picture of the material optical transitions (refractive index and absorption).

[0077] The illumination filters 14 can also be used to provide Fourier filtering of the beam from the illumination source 12. This could be used, for example, to present illumination that selects phase contrast on the disc or plate. If the disc or plate at a selected wavelength is in the anti-node condition (maximum field at the substrate surface), then phase contrast images can be acquired at that wavelength. If multiple wavelengths are used, then the phase contrast image can be combined with the quadrature images obtained at other wavelengths.

[0078] The illumination filters 14 can also be used to provide polarization of the light from the source 12 which can be informative if the molecules are oriented on the substrate.

[0079] The objective lens 18 could be any one of numerous objective lens systems known in the art (e.g., coverslip corrected; coverslip uncorrected; long working distance). The objective lens 18 is the imaging element in the system. It can be configured to work with or without coverslips. In the case of microfluidic systems, the objective should have a working distance that is compatible with the coverings over the microfluidic systems. In the

case of conventional 96-well plate, the objective lens should have a long working distance. This can sometimes reduce the magnification, but a large numerical aperture (NA) system can retain high magnification even for long working distance.

[0080] The substrate 34 could be composed of numerous materials (e.g., quadrature conditions: 120 nm oxide on silicon, 100 nm oxide on silicon, 80 nm oxide on silicon; SiN on silicon, anti-reflective (AR) coatings on glass, dielectric stacks on glass; Substrate formats: Quadraspec biological compact disc substrates, 96, 384, 1536- well plate substrates; and microfluidics). The substrate converts phase modulation to intensity modulation by interference effects set up by the substrate structure. This can be accomplished by a wide range of structures that have multiple layers ranging from a single layer to possibly hundreds.

[0081] One embodiment uses a substrate of thermal oxide grown on silicon. Thicknesses of 120 nm and 80 nm provide opposite quadrature at a wavelength of 635 nm. A thickness of 100 nm provides for phase-contrast imaging if a Fourier filter is used in the illumination and detection Fourier planes. Shifting of quadratures is also possible by choice of wavelength. Therefore, any multilayer substrate that produces partial reflections that may differ in phase by substantially $\pi/2$ will produce the appropriate phase-to-intensity conversion that is needed. An antireflection structure tuned near quadrature, or more generally dielectric stacks, can be used.

[0082] Substrate formats can be highly varied. A Quadraspec biological compact disc system format is possible, with direct imaging of protein spots in the wells. Or conventional 96-well plates can be used with protein spots printed onto an optically flat bottom that has been coated with dielectric layers that provide the quadrature condition. The substrates also can consist of microfluidic systems that deliver sample to the protein spots in real time. The molecular interferometric imaging process works when the system is immersed in water or biological fluids. The effects of the fluid matrix are cancelled by comparing the mass increase of a specific spot to land and also to non-specific spots. Therefore, the near-surface sensitivity of SPR and BioLayer Interferometry ("BLI") are not necessary because the full-field image allows reference values to be acquired simultaneously by which the matrix effects are subtracted.

[0083] The biolayers 32 can be structured in any of numerous ways known in the art. The biological molecules can be patterned on the disc in many possible configurations, the most common being spots, ridges and checkerboards. Periodic ridges enable Fourier image processing techniques in one-dimension, and checkerboard patterns allow Fourier image

analysis in two-dimensions. Alternating ridges of specific and non-specific molecules constitute an embodiment of differential encoding.

[0084] The stage 20 can also be structured in various embodiments (e.g., rotation; translation; dither). The stage motion enables normalization. Shifts of the stage 20 can take many formats that are chosen to be optimal for the different substrate formats. A rotation stage is perhaps most compatible with compact disc systems, while X-Y translation is most compatible with 96-well plates.

[0085] Dithering, which is another option for stage motion, is a periodic shifting back and forth. This might be used during kinetic binding experiments to better track the added mass. Dithering combined with synchronized pixel array image acquisition can be considered to be a type of pixel array lock-in approach.

[0086] The detection filters 22 can be any one of numerous detection filters known in the art (e.g., color; polarization; Fourier and image masks; phase contrast). The detection filters are placed before the pixel array 24. They may reside on image planes or Fourier planes. If the detection filters 22 are in the Fourier plane, they may include phase and amplitude masks. These masks can perform important functions such as phase contrast imaging. In this case, a $\pi/2$ mask on the Fourier plane can produce a phase contrast image on the pixel array 24.

[0087] Other detection filters that may reside on or off the image or Fourier planes would be wavelength and polarization filters that are matched to the respective illumination filters. These can allow multi-wavelength operation, for instance, or single wavelength operation. It would also be possible to place dichroic beamsplitters before the image detection to separate spatially images of different colors. Multiple dichroic beamsplitters would enable multiple different color images that could all be detected individually with individual cameras. Alternatively, a rotating filter wheel could sequentially switch color filters synchronized with the camera acquisition. This would enable multiple wavelength images to be acquired using only a single camera.

[0088] The pixel array 24 can be any of numerous image detectors known in the art (e.g., CCD; complementary metal oxide semiconductor ("CMOS"); pixel arrays; red, green and blue ("RGB"); megapixel; synchronization). Many formats are possible for the image detection. In one embodiment, the image detection is through a CCD or CMOS or pixel array device. Any device that has separate spatial channels to detect light at multiple locations on the image plane would be applicable. A pixel format having a high pixel density can be used, resulting in, for example, from 1 megapixel images up to 15 megapixel or greater images.

The "dead" space between pixels can be small. The pitch between pixels can also be small to reduce the requirements for high magnification.

[0089] Synchronization of the camera with an external trigger can be used to capture sequential images as some property is changed in the detection mode. For instance, synchronizing the camera with switching color filters, or synchronizing the camera with platform displacement or dither.

[0090] The camera 24 can be monochrome, using multiple color filters to acquire multicolor data - or the camera 24 can be a 3-color-channel array that detects red, green and blue individually. The oxide thickness of the substrate 34 can be changed to match the two quadrature conditions of the substrate to the red and blue channels on the camera, with the green channel representing the null condition in-between. This would allow full detection sensitivity for the red and blue, and enable full differential sensitivity for the green channel.

[0091] Advantages and improvements of the methods of the present invention are demonstrated in the following examples. The examples are illustrative only and are not intended to limit or preclude other embodiments of the invention.

[0092] Images of proteins on thermal oxide on silicon in the quadrature condition using a color filter on a conventional microscope have been acquired. These images were near the quadrature condition. First and second images were acquired with the platform displaced in-between acquisitions. The differential composite exhibited high sensitivity to protein and low sensitivity to background effects.

[0093] A direct image under 40x magnification of a protein is shown in Figure 9A. The protein was IgG printed on 120 nm oxide on silicon. The spot was printed using a Scienion printer with approximately 100 picoliters of liquid volume. The substrate is an in-line quadrature Quadraspec biological compact disc with functionalized surface chemistry. The full range of the color bar is approximately 4 nanometers. The image was acquired with a 12-bit CCD camera. The intensity modulation caused by the protein is generally a few percent. The protein height is approximately a nanometer. The brighter tail on the lower left is the wash-off tail which is several nanometers high. The variability in the image is mostly caused by inhomogeneous illumination and also by dust in the optics. The background variability is smaller than, but still comparable to, the magnitude of the protein signal.

[0094] The protein spot after execution of the platform shift and the calculation of the differential composite image is shown in Figure 9B. Most of the background variability is removed by the normalization procedure of Eq. (10). The protein heights in the image are several nanometers.

[0095] Figure 10 shows a high resolution protein image of a uniformly printed 120 micron diameter protein spot. The protein height is approximately 1 – 2 nanometers. The full range scale is -2 nm to 2 nm.

[0096] A photo gallery of many differential composite images for many types of spot morphologies is shown in Figure 11. The protein spots are all approximately 100 microns in diameter. The images were acquired from many different wafers using many different chemistries. The protein spot heights in all cases are from about half a nanometer to several nanometers.

[0097] Figure 12 shows a pseudo three-dimensional image of surface morphology of a printed spot with a pronounced outer ring. The high circular rim is caused by preferential protein deposition as the spot evaporates. The ring height is approximately 0.7 nm.

[0098] The local background normalization procedure using shearing interferometry removes the spatial 1/f noise. The remaining noise in the resulting differential surface profile are the temporal 1/f noise (which is the long-term system drift), and the noise from the CCD camera. When the measurement time is short compared to the system drift, then the CCD is operating close to full-well depth, and the measurement of the differential surface profile is shot-noise limited.

[0099] Repeatability experiments were performed in which pixel variability was measured as a function of the number of frames that were acquired and averaged. The height repeatability (standard deviation) is plotted in Figure 13 as a function of the number of acquisitions for both 40x and 4x objective magnification. The standard deviation of the differenced images decreases inversely with the square root of the number of acquisitions up to approximately 1024 images. For more images than this, long-term drift begins to dominate, representing 1/f noise. The minimum standard deviation was 20 picometers per pixel. The fluctuations for 4x are not much higher. The pixel size in the case of 40x is 0.5 microns, and for 4x is 5 microns. When the platform shift is used to normalize the pixel values, the standard deviation increases by about a factor of 3 to 60 picometers. The equivalent number of IgG molecules that this corresponds to is approximately 100 molecules. This is illustrated in Figure 14, in which the pixel-to-pixel fluctuations are at the level of approximately 100 molecules on the edge of the printed protein spot.

[00100] Further repeatability experiments were performed with the experimental embodiment using the CCD camera described previously. Because of the shot-noise-limited nature of the CCD detection, we average many images together to obtain a larger photon exposure to reduce the relative shot-noise. Figure 15 shows the effect of data averaging on

the detection noise of the surface height profile. The detection noise is obtained by differencing consecutively-collected images (with averaging) and calculating the standard deviation of the difference. The curves for different magnifications are separated because of different intensity-to-height conversion ratios. The absolute intensity noise at different magnifications is comparable, because it only arises from the CCD camera and is not related to the actual optical system. The noise decreases as the square root of the number of averages taken, suggesting that the noise is random and uncorrelated, which is another property of shot-noise. When the integration time becomes too long, long-term system drift begins to dominate, which increases the measurement noise. The noise is a minimum around 12 pm at 4096 averages for 40x magnification. We typically use 128 averages at a frame rate of 4 fps, which takes 30 seconds for the acquisition of one image. If a faster CCD, or a CCD with a larger well depth, is used it would be possible to reduce the noise even further, as more photons can be collected in the same data acquisition time.

[00101] The metrology limit of molecular interferometric imaging is calculated using the minimum of the detection noise, which is 12 pm per pixel with 40x magnification at 4096 averages at the lateral resolution of 0.4 μm. The height sensitivity of 12 pm corresponds to 2 attogram of protein per pixel for a protein density of 1.3 g/cm^3 is assumed. This is approximately 8 antibody molecules with a typical size of 150 kD, which is close to single-molecule detection. The scaling mass sensitivity is calculated by dividing the minimum detectable mass by the square-root of the measurement area, and is 5 fg/mm in the metrology limit.

[00102] This metrology limit is obtained under ideal conditions, without dismounting or moving the disc. Therefore, this limit is not achieved in practical assays in which the disc needs to be dismounted for sample incubation. When the disc is dismounted and remounted, the random position shift of the sample causes the derivative of the surface roughness to influence the measurement and becomes the dominant source of measurement uncertainty. As a result, in a practical assay under our current experimental protocol of 128 averages, the measurement uncertainty increases to about 100 pm/pixel. The scaling mass sensitivity is inversely proportional to pixel resolution, and for practical assays under 7x, 20x and 40x magnification, the scaling mass sensitivity is 200, 70 and 40 fg/mm, respectively. Higher magnification results in higher sensitivity, but increases the scanning time.

[00103] Embodiments of the present invention can also operate under water. The protein differential composite image is shown in Figure 16 under the two conditions of dry

and wet. The protein was under a glass coverslip. Water was introduced between the slip and the disc surface. The protein is still visible, with approximately a factor of 3 reduction in the signal intensity. At the same time, dust and other background noise also decreased by about a factor of 3 keeping the signal-to-noise ratio approximately constant. Detection sensitivity is set by the signal-to-noise ratio. Therefore, operation of the molecular interferometric imaging under water is feasible. This enables kinetic capture experiments in which binding could be tracked in real time. To detect real time binding, either the platform is dithered with synchronized image acquisition, or else successive images would be differenced and normalized to detect the binding.

[00104] These data also demonstrate the ability to use the known refractive index of water to measure the refractive index of the protein. The protein signal under water is still a positive signal. This requires that the refractive index of the protein be larger than the refractive index of water. The refractive index of the protein is calculated by solving the equation:

$$\frac{n-1}{n-1.33} = \frac{\Delta I_{dry}}{\Delta I_{wet}} \qquad (11)$$

The refractive index measured for the protein layer in this way is approximately n = 1.5.

[00105] The capability to directly image through water using molecular interferometric imaging enables real-time binding experiments. A simplified diagram of the experimental arrangement is shown in Figure 17. The optical arrangement is similar to that of Figure 3, and for clarity only the objective lens 118 is shown. However, now a sample 130 is to be characterized that has an active flow of liquid in the direction of arrow 133 over antibody spots 134 on a support layer 138. The lower white part of the spots 134 represents the antibody and the upper dark part of the spots 134 represents the captured analyte. The support layer 138 can be the top surface of a substrate or oxide layer.

[00106] The imaging is performed through a top glass coverslip 136 and through the liquid. The liquid is a potential source of background signal because it contains the analytes that are being captured out of solution by the antibody spots 134. However, the captured mass is enhanced relative to the background analyte by the anti-node condition that is at the surface of the support layer 138. The field strength is twice as high at the protein spot 134 compared to the average over the liquid volume. Furthermore, in molecular interferometric imaging, continual image-pair acquisition is taking place that compares the mass over the spot 134 to the mass captured by adjacent land 138. The overlying fluid remains the same in both images and hence is subtracted. Another approach to ameliorate the background in the

liquid could be to periodically flush the system with buffer, during which image pairs are acquired. In this case, the overlying liquid is free of the analyte. A combination of both approaches might give the best balance in terms of sensitivity to bound analyte.

[00107] The in-line approach also makes it possible to interrogate the proteins without going through the liquid. One embodiment of this is shown in Figure 18. The imaging geometry is the same as that of Figure 17, but now the light passes through the upper glass slide 238 that carries the antibody spots and the bound analyte 234. The in-line quadrature condition is established by appropriate dielectric layers 232. A top reflection can be the reference wave, and the reflection off the protein-carrying surface can be the signal wave. The addition of mass on the protein spot 234 alters the phase of the reflected light that is detected through the in-line quadrature interfeormetry at the camera. This approach has the advantage that the light does not pass through the liquid layer containing the analyte.

[00108] Figure 19 is a graph of experimental data from real-time binding showing an increase in the spot height for the specific spots, and a decrease in the spot height for the non-specific reference spots. The decrease in spot height for the non-specific reference spots is due to wash-off. The time between frames is 40 seconds. The analyte concentration was 40 ug/ml. During the collection of 28 images (1,080 seconds or 18 minutes) the relative binding on the specific spots increased from approximately 0.0001 to 0.0020 while the relative binding on the non-specific spots decreased from approximately 0.0001 to -0.0004.

[00109] The sensitivity of the molecular interferometric imaging approach can be enhanced by increasing the data acquisition rate, especially with respect to disc translation from spot to spot. A simple embodiment is to utilize a slowly spinning disc or translating plate as shown in Figure 20. The pixel array of the system has a field of view 250 and the sample has a protein spot 254. In part (A) of Figure 20, the camera shutter is opened and closed on a time scale that is short relative to the motion of the protein spot 254. This results in a multiple exposure of the same protein spot 254 as it travels across the field of view 250. In the case shown in Figure 20(A), an image with six multiple exposures of the protein spot are captured at different positions in the field of view 250. For normalization purposes, the same operation can be done for the adjacent land as shown in part (B) of Figure 20. In the case shown in Figure 20(B), an image with six multiple exposures of the land, which is substantially clean and uniform, is captured at different positions in the field of view 250. Different magnifications can be used to capture more or less protein spots in the field of view.

[00110] Each exposure is of the same protein spot 254, providing averaged detection statistics, and the multiple exposure image of the protein spot is referenced to a multiple exposure image of different parts of the land, providing averaging over the land topology which can be a limiting factor in single-pair molecular interferometric imaging. This approach would not necessarily need a larger memory, because the shutter could open and shut many times prior to reading out the digital image. The data in this case is a repeated exposure. Many images of the spot and land are acquired in only one multiple exposure image.

[00111] Another embodiment that utilizes a continuously spinning disc or translating plate, and takes the last embodiment to its limiting behavior, is time-lapse exposure while the disc is continuously spinning or plate is continuously moving as shown in Figure 21. The pixel array of the system has a field of view 260 and the sample has a protein spot 264. In part (A) of Figure 21, the camera shutter is opened when the spot 264 is at position 266 at the edge of the field of view 260. The shutter remains open while the protein spot 264 crosses the field of view 260 and finally closes when the spot 264 reaches position 268 at the other side of the field of view 260. For normalization purposes, the shutter remains open for the same time period as the adjacent land as shown in part (B) of Figure 16 traverses the field of view 260 in the direction of arrow 262.

[00112] While the spot 264 is moving across the field of view 260, the pixel array records an average intensity that is a combination of the protein spot 264 and the adjacent land on the trailing side and appears as a "swath". The average intensity over the swath provides a means for averaging spatial illumination drift, which can be a limiting factor in molecular interferometric imaging.

[00113] Rapid acquisition of the reference surface improves the results of the molecular interferometric imaging system. The idea of disc translation, taken to the limiting case of having the disc spin, is one type of approach, but other approaches are also possible. The purpose of the reference surface in molecular interferometric imaging is to provide intensity normalization. This is a relatively easy requirement that is much simpler than the reference surfaces that are required for non-common-path interferometers in which the reference surface distance must be stabilized to within a small fraction of a wavelength. Therefore, all that is needed is a means of introducing the reference surface as a separate image to be acquired.

[00114] One embodiment is to have a high-speed mirror that rapidly switches back and forth between a protein spot and a physically separated reference surface. The image acquisition by the camera can be synchronized with the mirror motion.

[00115] Another embodiment is to have a mirror on a spinning disc that is between the protein layer and the objective lens. The disc would have a clear aperture to image the protein spot, then the mirror moves between the lens and the protein spot. A reference image is acquired at the moment the mirror is between the lens and the protein spot. A similar embodiment uses an oscillating galvonometer that switches the image between the reference surface and the protein spot.

[00116] Figure 22 shows an embodiment that requires no moving parts. This embodiment uses beam polarization control by passing the beam through an electro-optic modulator in a half-wave configuration. The polarization is switched back and forth between orthogonal polarizations. The polarized beam passes through the objective lens 278 and enters the polarizing beam splitter 272 which redirects the illuminating beam back and forth, depending on its vertical and horizontal polarization either to the protein spot 274, or to the reference surface 276. Image acquisition would be synchronized with the polarization.

[00117] To demonstrate the potential of molecular interferometric imaging in performing highly-multiplexed assays, we performed a multiplexed reverse-phase assay in which immobilized rabbit and mouse IgG were incubated against anti-rabbit and anti-mouse IgG in solution. A 120 nm silicon oxide on silicon wafer was plasma cleaned and separated into wells by hydrophobic ink. The silicon oxide surface was then functionalized with the di-isocynate coating. Each well was printed with 64 protein spots that form 16 2x2 unit cells that have mouse IgG on one diagonal and rabbit IgG on the other. For the experiment 64 wells were selected and were incubated with samples that had 64 different concentration combinations of anti-rabbit IgG from goat (Sigma), anti-mouse IgG from goat (Sigma) and albumin from bovine serum (BSA) (Sigma). All samples were prepared in 10 mM pH 7.4 PBS buffer. Each protein had four different concentrations and all permutations of these concentrations produced 64 different three-component sample mixtures. Together with the 2 different analytes printed on the disc, this experiment is a 128-plex immunoassay. The concentrations of anti-rabbit IgG were 0, 1, 10 and 100 ng/mL. The concentrations for anti-mouse IgG were 0, 10, 100, 1000 ng/mL. The concentrations for BSA were 0, 10, 100 and 1000 μg/mL. The disc was incubated statically for one hour, then it was rinsed with distilled water and blown dry by nitrogen.

[00118] The 64 wells selected for this experiment were scanned with 7x magnification before incubation and scanned again after the one-hour static incubation. The data were analyzed in the same way as described before. For each spot, the post scan and pre scan data were registered by cross-correlation, and shifted with linear interpolation. Then the two images were differenced to obtain a difference image of protein height change for each pixel of the spot, and the difference image was histogramed and fit to a Gaussian distribution to extract the mean height change for the spot. The 32 mouse and rabbit spots in each well were averaged together to obtain the assay response for each well.

[00119] The result of the analysis is shown in Figure 23 as a color map of the assay responses across the 64 wells. The responses of the mouse spots are plotted in red, with increasing concentrations of anti-mouse downward and varying concentrations of BSA and anti-rabbit across to the right. The responses of the rabbit spots are plotted in green, with increasing concentrations of anti-rabbit moving right in the horizontal direction with varying concentrations of BSA and anti-mouse downward. The intensity of the color represents the magnitude of the protein binding. For both the mouse and rabbit assay, the binding of protein increases with increasing concentration, as can be seen from an increasing brightness of the color. The presence of a high concentration protein background (BSA) does not have significant effect on the binding, and there is no systematic trend within each analyte concentration.

[00120] The two responses were averaged over the BSA concentration and combined into a single matrix in combined color, in which equal intensity of red and green produces yellow (bottom right). The intensity of the color shows the strength of the protein binding. In this matrix, the highest concentration well for both analyte is yellow, showing that the binding of anti-mouse and anti-rabbit were similar. The color turns more red going left, and more green going up, and with a decreasing intensity for the lower concentrations. The limit of detection (LOD) of this 128-plex assay was approximately 50 ng/ml per well. The sensitivity was limited by spot-to-spot and by well-to-well variability across the disc. Much more sensitive assays are possible in a monolithic array format without the hydrophobic barriers, which we demonstrate next in an assay for prostate-specific antigen.

[00121] Prostate cancer (PCa) accounts for 10% of all deaths from cancer. A major focus of prostate cancer research has been the early detection of PCa using serum biomarkers. The most commonly used biomarker for prostate cancer is prostate specific antigen (PSA), a member of the kallikrein family. PSA in seminal fluid has a concentration of 0.5 mg/mL to 2.0 mg/mL. We tested the sensitivity of our detection system with a sandwich assay of PSA.

In a sandwich assay, a capture antibody is immobilized onto the substrate to capture the antigen in a sample. Then it is incubated against a secondary antibody that binds to the captured antigen to boost the binding signal. For this experiment, a 120 nm silicon oxide disc was plasma cleaned and functionalized with the di-isocynate surface coating. Then it was printed with more than 25,000 spots in a 256x100 radial grid pattern. The tangential distance between two spots was $2\pi/256$, and the radial separation of spots was 0.3 mm. The spots were printed in 2x2 unit cells of target and reference, with goat anti-PSA antibody (Biospacific) as target in one diagonal of the unit cell, and goat anti-rabbit IgG (Sigma) as reference in the other diagonal. The concentrations of the print solutions were 100 μg/mL.

[00122] The entire disc was then incubated against 10 ng/mL of PSA antigen (Fitzgerald Inc.) spiked into a high-concentration protein background of 2 mg/mL BSA on an orbital shaker (VWR) for 3 hours. The solution was prepared in 10mM pH 7.4 PBS buffer, with 0.05% Tween 20. The 3-hour incubation on orbital shaker removes potential mass transport problems of surface capture and drives the reaction to equilibrium. After incubation with antigen, the disc was rinsed with distilled water and blown dry by nitrogen, and protein spots were scanned with molecular interferometric imaging under 20x magnification. The disc was then incubated with 100 ng/mL of goat anti-PSA (Biospacific) in PBS buffer with 0.05% Tween 20 on orbital shaker for 30 minutes. After rinsing with distilled water and dried by nitrogen, the same protein spots were scanned again under 20x molecular interferometric imaging.

[00123] The pre-scan and post-scan of the protein spots were registered and differenced, and the histograms of the differences for a single pair of spots are shown in Figure 24, which shows the binding of the secondary antibody to the captured antigen. The broad distributions in the difference are caused by inhomogeneous spot morphology. Although the distributions are not well separated, more than 15,000 pixels were used in the histograms for each spot, and therefore the standard error for the distributions is reduced by a factor of 120. The resulting height change for the target spot is 0.613 ± 0.005 nm, and the height change for the reference spot is -0.195 ± 0.005 nm. The negative value for the reference spot is caused by the wash-off. The signal-to-noise ratio for a single pair of spots is 160:1. Because the disc was incubated with 10 ng/mL of PSA, this extrapolates to a concentration detection limit of 60 pg/mL, which is well below the normal concentration of PSA in human sera. The detection was performed in a high concentration protein background of 2 mg/mL BSA, which did not affect the assay significantly. Because a single

pair of spots were used for this analysis, a disc that is printed with 25,000 spots would be able to perform more than 10,000 assays, each with a detection limit of 60 pg/mL.

[00124] Detection of Interleukin-5 (IL5) cytokine through sandwich assays was performed using molecular interferometric imaging. The cytokine IL5 is an important signaling protein in the immune system. For this experiment, both di-isocynate and butyraldehyde surface chemistries were used, and capture antibodies were immobilized by either direct printing or by binding to protein A/G that was printed directly onto the surface. Discs with 120 nm oxide were used for this experiment, and each disc was separated into 96 independent wells by hydrophobic pads. The surfaces of the discs were functionalized by either di-isocynate or butyraldehyde chemistry, and then printed with protein spots. Each well was then printed with 64 protein spots that formed 16 2x2 unit cells of target and reference spots on opposite diagonals. On half of each disc, the target spots were directly printed with capture antibody (BD Biosciences), and on the other half of the disc, the target spots were printed with protein A/G. The wells that were printed with protein A/G were incubated with the capture antibody. After the immobilization of the capture antibody, different wells of the discs were incubated statically for 2 hours with 3 different concentrations of IL5: 0, 50 pg/mL and 1 ng/mL. The discs were then scanned with molecular interferometric imaging under 20x magnification. After the scan, the wells were incubated statically for 1 hour with secondary antibody at a concentration of 100 ng/mL. The discs were scanned again after the incubation of secondary antibody.

[00125] The pre-scan and post-scan were registered and differenced to obtain the binding signal of the secondary antibody to the captured antigen. The height change differences for each pair of target and reference spots were calculated, and for each concentration the differences of all the pairs were averaged together. The results of the analysis for the direct-printed antibodies on the di-isocynate coated disc are shown in Figure 25. The error bars on the response curve are set by the standard error of the pair responses. At 50 pg/mL, the binding signal is distinguished from 0 by the error bar. The average height change at 50 pg/mL is 60 pm, with an error bar of 30 pm.

[00126] The above results were for the directly-printed capture antibody. The same analysis was performed for the protein A/G immobilized capture assays. After incubating with the secondary antibody, the 0-concentration wells showed a large height increase, whereas in the higher concentration wells the height increase was much smaller. The results are plotted in Figure 26 as the maximum binding to A/G at zero concentration minus the spot response vs. increasing antigen concentration. This suggests that under this experimental

condition, the IL5 competes with the immobilized protein A/G to bind with the secondary antibody. Therefore it behaves as a competitive assay in which higher concentrations of antigen bind more secondary antibody so that less secondary antibody is bound to the protein A/G spot. Under this condition, the balance of the reaction is highly sensitive to the change in antigen concentration. At 50 pg/mL the response difference for the butyraldehyde-coated disc is 250 pm with a standard error of 20 pm. Similar results were obtained for the di-isocynate coated disc, although with a smaller magnitude. The projected concentration detection limit for this competitive assay of IL-5 against protein A/G is 3 pg/mL.

[00127] The direct imaging character of molecular interferometric imaging enables real-time binding measurements in which the surface is imaged through the incubant. This gives it the capability of observing antibody binding in solution in real-time, in a manner similar to surface plasmon resonance sensors. The main difference is that surface plasmon resonance probes the interface using an evanescent field, while in molecular interferometric imaging the optical field penetrates the full fluid thickness above the surface. However, if the fluid sample is homogeneous and non-turbid, it causes no degradation in the sensitivity of the measurements other than a decrease in the protein contrast given by (np-nw)/(np-1) = 0.25. Although the probe beam travels through the fluid, if the fluid moves faster than analyte is depleted, only the incremental mass binding at the surface is detected because it is a differential measurement over time. One drawback of this approach relative to surface plasmon resonance is that if the fluid is static, then the differential signal is reduced by the depletion of analyte above the antibody spot. For this reason, we use actively flowing sample in all our experiments. This has not only the advantage of sweeping fluid away from the spot before it is depleted, but also enables the surface binding kinetics to be free of transport limitations.

[00128] In the kinetic experiments using molecular interferometric imaging, a well on a disc is covered with a 0.17 mm thick microscope cover glass. Fluid was injected under the cover slip on one side, and drained from the other. The cover glass was attached by double-sided tape to make the height of the flow cell approximately 100 microns. The flow rate of the fluid was controlled by a valve, and was typically about 100 μm/sec for the experiments. The protein spots were imaged directly through the cover slip. In this type of real-time detection, the disc is not shifted, and the data that are taken at different times are normalized by the first image to remove the spatial 1/f noise. The slow temporal drift in the illumination

background is removed by software. This measurement obtains differential surface height change as a function of time.

[00129] As a proof of principle, the real-time binding of rabbit IgG against goat anti-rabbit IgG with secondary amplification was measured. For this study 6 wells were printed with goat anti-mouse IgG (Sigma) and goat anti-rabbit IgG (Sigma), and were incubated against two different concentrations of rabbit IgG, at 2 μg/mL and 20 μg/mL, with different exposure times of 1 min, 3 min and 10 min. They were then incubated against 20 μg/mL of anti-rabbit IgG as the secondary antibody, and the resulting signal change for the specific spots is plotted in Figure 27A. Longer incubation time caused higher captured antigen concentration on the specific spots, and caused a faster height increase when incubated against the secondary antibody. The oscillations in the real-time binding are caused by the drift of interference fringes from the light reflected from the glass cover slip. Because the relative intensity change caused by the protein binding is on the order of 0.1% of the total intensity, the interference fringes cause a non-trivial effect. The effect of the interference fringes can be reduced by improving the attachment of the cover slip, and the mechanical stability of the flow system. They can be further reduced by using anti-reflection coated cover slips.

[00130] The saturation height of the binding curves in Figure 27A is proportional to the captured antigen, which is plotted in Figure 27B as a function of the amount of antigen exposure. Longer exposure results in higher saturation height and higher reaction rate.

[00131] The entire process of real-time binding to printed protein G spots is shown in Figure 28. The vertical axis is the height change of the protein G spots, and the error bar is set by the standard error of 20 different protein G spots in the field of view. An 84-well disc was printed with protein G, and one well was selected for the real-time binding experiment. PBS buffer was first flowed through the flow cell, which sets the baseline of the measurements and drives the protein spots to equilibrium. Then the fluid was switched to 20 μg/mL of anti-rabbit IgG. The anti-rabbit IgG was captured onto the protein G spot, and saturated at a height of 3 nm. Then 20 μg/mL of rabbit IgG was flowed through the system. The immobilized anti-rabbit IgG captured rabbit IgG in the solution, and gained 1 nm of height. Finally 20 μg/mL of anti-rabbit IgG was applied again into the system and bound with the captured rabbit IgG. The binding increased the spot heights by 5 nm. All solutions were prepared in 10 mM PBS buffer, and PBS buffer was briefly applied during each change in protein solution to make sure that the protein solutions did not mix together.

[00132] The successive step heights after each protein application in Figure 28 relate to the biological or chemical activity of the immobilized chemistry and capture molecules. The first step is caused by the binding of the Fc regions of the antibody to the printed protein G. This step height is approximately 3 nm corresponding approximately to a half-monolayer of captured antibody. The second step is caused by presenting antigen to the bound antibody. This step height is only about 1 nm, suggesting that only about one in three antibody molecules is capturing antigen. The final step height is caused by the sandwich secondary antibody with a much higher step height of approximately 6 nm. This large step suggests that there are approximately 6 antibodies attaching to each captured antigen. This secondary amplification may be possible because the secondary antibody is a polyclonal antibody that can bind to more than one epitope on the antigen. It is further possible to produce polymer chains of polyclonal antibodies with the antigen acting as the cross-linker. Considerable future work is needed to study these effects, and to verify that the overlying fluid is not participating significantly in the observed intensity changes.

[00133] While exemplary embodiments incorporating the principles of the present invention have been disclosed hereinabove, the present invention is not limited to the disclosed embodiments. Instead, this application is intended to cover any variations, uses, or adaptations of the invention using its general principles. Further, this application is intended to cover such departures from the present disclosure as come within known or customary practice in the art to which this invention pertains and which fall within the limits of the appended claims.

We claim:

1. A molecular interferometric imaging system for detecting an analyte in a sample, the molecular interferometric imaging system comprising:

an illumination source providing a beam of radiation;

a pixel array comprising a plurality of pixels for detecting radiation at a plurality of locations in an image plane to produce an image comprising a plurality of pixel readings;

a biolayer designed to react to the analyte when the biolayer comes in contact with the sample;

a substrate, the biolayer being located on the substrate, the substrate being designed to convert phase modulation into intensity modulation which can be detected and imaged directly by the pixel array;

a reference surface;

an image switching means for switching between a first position in which the beam provided by the illumination source is incident on the biolayer and a reflected sample beam is produced which is directed to the pixel array to generate a sample image, and a second position in which the beam provided by the illumination source is incident on the reference surface and a reflected reference beam is produced which is directed to the pixel array to generate a reference image; and

a processing means for producing a composite image using the sample image and the reference image for illumination normalization.

2. The system of claim 1, wherein the substrate comprises a support layer and a spacer, the thickness of the spacer being selected to produce an in-line quadrature condition.

3. The system of claim 2, wherein the spacer acts as the reference surface.

4. The system of claim 2, wherein the support layer is silicon and the spacer is a thermal oxide layer.

5. The system of claim 4, wherein the thickness of the oxide layer is 120 nm.

6. The system of claim 1, wherein the substrate acts as the reference surface, and the image switching means is a stage for moving the substrate and the biolayer between the first position and the second position.

7. The system of claim 1, wherein the biolayer comprises a plurality of separate spots deposited on the substrate with the substrate being exposed to separate the plurality of separate spots.

8. The system of claim 7, wherein the substrate acts as the reference surface.

9. The system of claim 1, wherein the processing means computes a difference between the plurality of pixel readings of the reference image and the plurality of pixel readings of the sample image on a pixel by pixel basis.

10. The system of claim 1, wherein the illumination source is a laser tuned to a desired frequency, the desired frequency being selected such that the reflected radiation from the substrate and the radiation from the biolayer are in an in-line quadrature condition.

11. The system of claim 1, further comprising an illumination filter.

12. The system of claim 11, wherein the illumination source produces a multi-frequency beam and the illumination filter filters the beam such that only a desired frequency passes through the illumination filter, the desired frequency being selected such that the reflected radiation from the substrate and the radiation from the biolayer are in an in-line quadrature condition.

13. The system of claim 11, wherein the illumination source produces a multi-frequency beam and the illumination filter filters the beam such that only a first wavelength and a second wavelength pass through the illumination filter, the first and second wavelengths being selected such that the reflected radiation from the substrate and the radiation from the biolayer are in an in-line quadrature condition, the first wavelength being different from the second wavelength.

14. The system of claim 11, further comprising a detection filter, the detection filter being matched to the illumination filter to produce a desired property in the beam incident on the pixel array.

15. The system of claim 1, further comprising a beam splitter, the beam splitter directing the beam from the illumination source to the image plane and directing the reflected beam from the image plane to the pixel array.

16. The system of claim 1, further comprising a trigger to synchronize image collection with switching by the image switching means.

17. The system of claim 16, wherein the image switching means is a mirror that moves between the first position to view the biolayer and the second position to view the reference surface.

18. The system of claim 16, wherein the image switching means is a spinning disc that includes an aperture, the spinning disc being in the first position when the biolayer is visible through the aperture and the spinning disc being in the second position when the biolayer is not visible through the aperture.

19. The system of claim 16, wherein the image switching means is a polarizing beam splitter that switches back and forth between orthogonal polarizations, the polarizing beam splitter being in the first position when the polarization setting directs the beam to the biolayer and the polarizing beam splitter being in the second position when the orthogonal polarization setting directs the beam to the reference surface.

20. The system of claim 1, further comprising a trigger to synchronize image collection with changing of properties of the beam incident on the pixel array.

21. The system of claim 1, wherein the biolayer is immersed in a fluid during collection of the sample image.

22. The system of claim 21, wherein the fluid is actively flowing during collection of the sample image.

23. The system of claim 1, wherein the image switching means is a stage, the stage moving between the first position in which a first set of pixels of the plurality of pixels is exposed to the biolayer, and the second position in which a second set of pixels of the plurality of pixels is exposed to the biolayer, there being no intersection between the first set of pixels and the second set of pixels.

24. A method of molecular interferometric imaging for detecting an analyte in a sample using a pixel array comprising a plurality of pixels for detecting radiation at a plurality of locations in an image plane, and a substrate designed to convert phase modulation into intensity modulation which can be detected and imaged directly by the pixel array, the method comprising:

exposing a biolayer that is deposited on the substrate to the sample, the biolayer being designed to react to the analyte when the biolayer comes in contact with the sample;

positioning an image switching means in a first position;

illuminating the biolayer with a radiation source to produce a sample beam;

capturing the sample beam in a sample image using the pixel array;

positioning the image switching means in a second position;

illuminating a reference surface with the radiation source to produce a reference beam;

capturing the reference beam in a reference image using the pixel array;

computing a composite image using the sample image and the reference image for illumination normalization.

25. The method of claim 24 wherein the sample image exposes a first set of pixels to the biolayer and exposes a second set of pixels to the reference surface, and the reference image exposes the first set of pixels to the reference surface and exposes the second set of pixels to the biolayer, and the computing a composite image step comprises:

subtracting the pixel readings from the sample image from the pixel readings of the reference image.

26. The method of claim 24 wherein the sample image exposes a first set of pixels to the biolayer and exposes a second set of pixels to the reference surface, and the reference image

exposes the first set of pixels to the reference surface and exposes the second set of pixels to the biolayer, and the computing a composite image step comprises:

computing, on a pixel by pixel basis,

$$I_{Diff} = 2\frac{(I_A - I_B)}{(I_A + I_B)} \quad (4)$$

where I_B are the pixel readings from the sample image and I_A are the pixel readings from the reference image.

27. The method of claim 24, further comprising filtering the radiation source such that only a desired set of wavelengths are captured in the sample image and the reference image.

28. The method of claim 24, further comprising rotating the image switching means to move between the first position and the second position.

29. The method of claim 24, further comprising synchronizing the capturing of the sample image and the reference image with movement of the image switching means.

30. The method of claim 24, wherein the sample image is collected while the biolayer is immersed in a liquid.

31. The method of claim 30, wherein the sample beam passes through the liquid.

32. The method of claim 30, wherein the sample beam does not pass through the liquid.

33. The method of claim 24, wherein

capturing the sample image comprises capturing a multiple exposure image of the biolayer as it traverses the field of view of the pixel array, and

capturing the reference image comprises capturing a multiple exposure image of the reference surface as it traverses the field of view of the pixel array.

34. The method of claim 24, wherein

capturing the sample image comprises capturing a time lapse image of the biolayer as it traverses the field of view of the pixel array, and

capturing the reference image comprises capturing a time lapse image of the reference surface as it traverses the field of view of the pixel array.

Figure 1

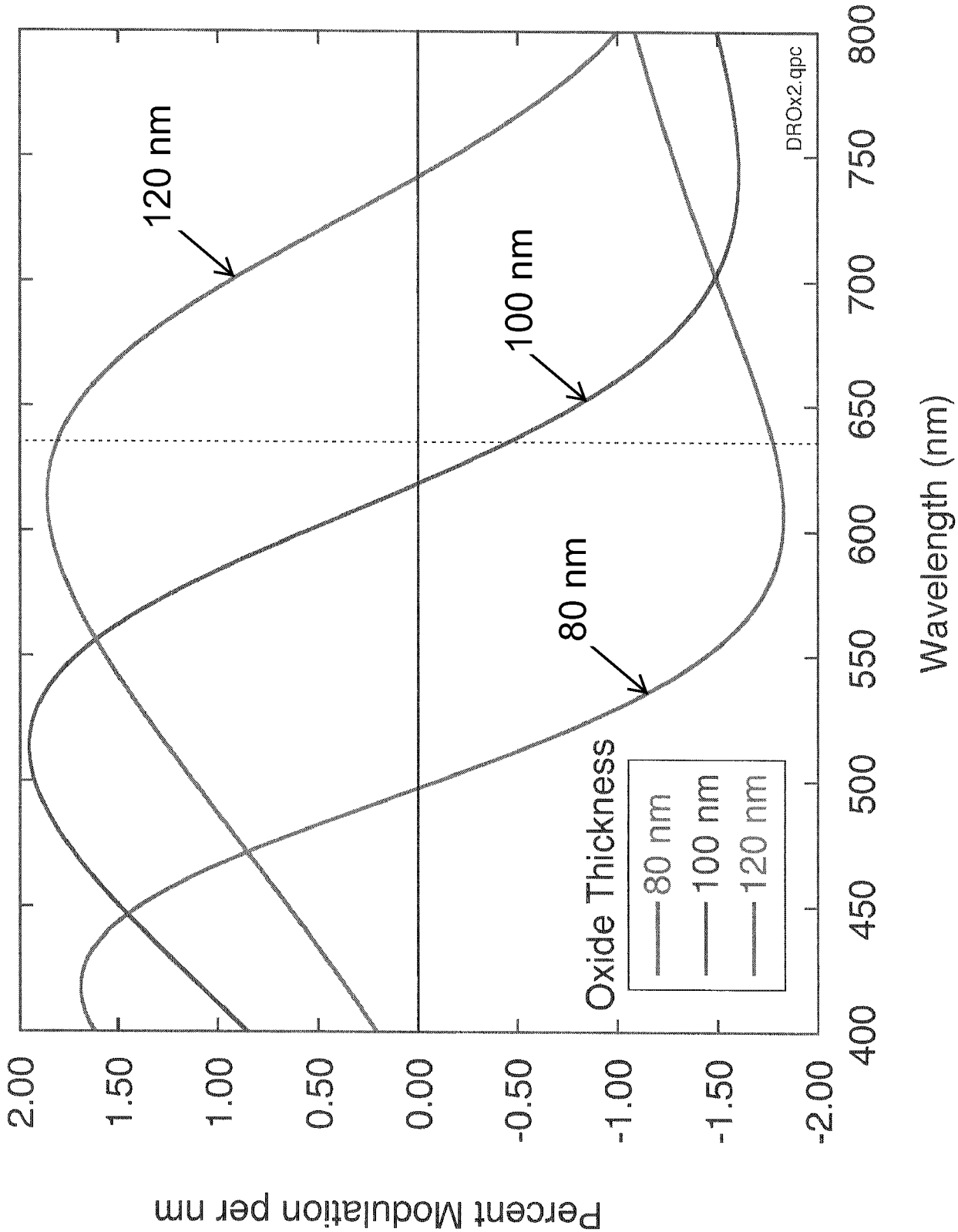
Response to Biolayer
Percent Modulation per nm
Wavelength (nm)
120 nm
100 nm
80 nm
Oxide Thickness
80 nm
100 nm
120 nm
DROx2.qpc
2.00
1.50
1.00
0.50
0.00
-0.50
-1.00
-1.50
-2.00
400
450
500
550
600
650
700
750
800

Figure 2

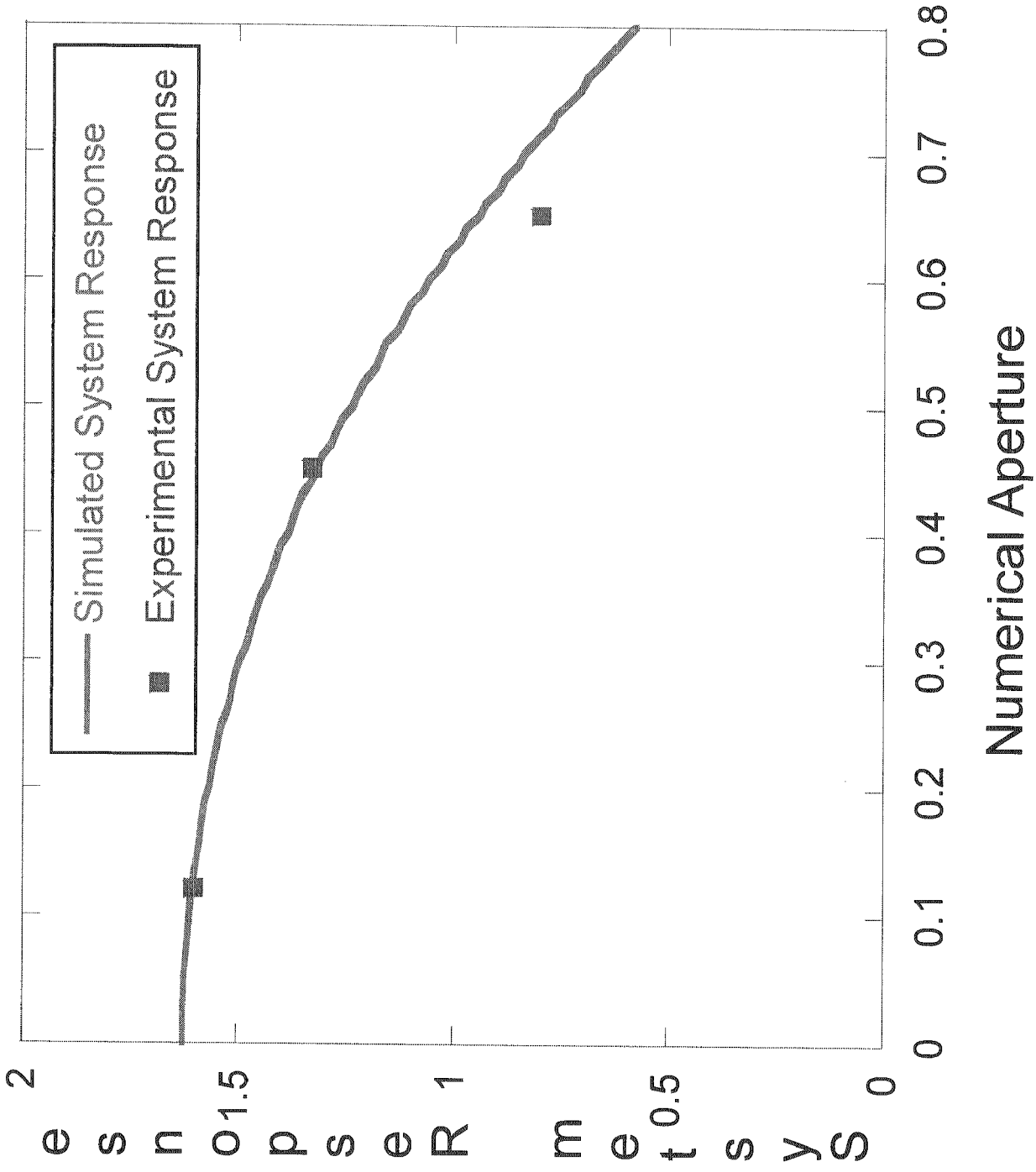
Simulated System Response
Experimental System Response
System Response
0
0.5
1
1.5
2
0
0.1
0.2
0.3
0.4
0.5
0.6
0.7
0.8
Numerical Aperture

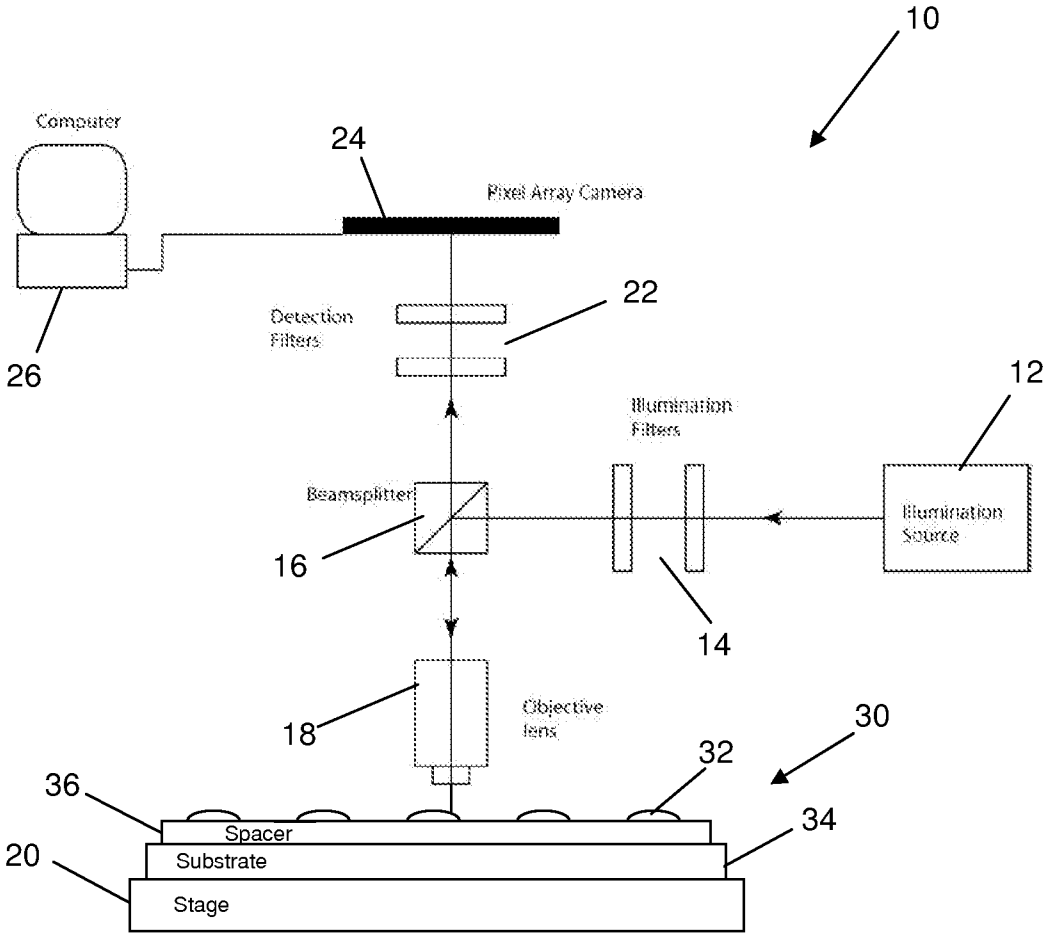
10
Computer
24
Pixel Array Camera
22
Detection Filters
26
12
Illumination Filters
Beamsplitter
Illumination Source
16
14
18
Objective lens
30
32
36
34
Spacer
Substrate
20
Stage

Figure 3

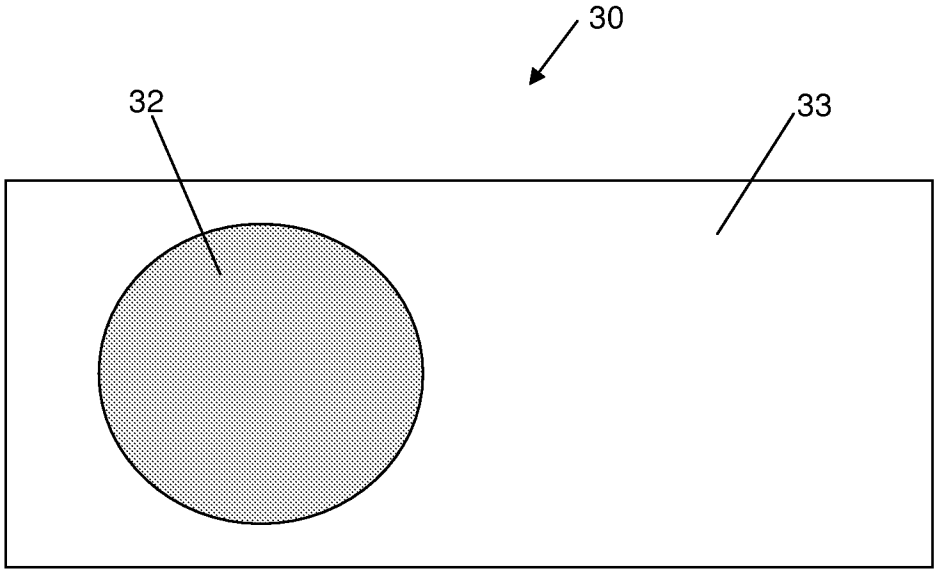

Figure 4

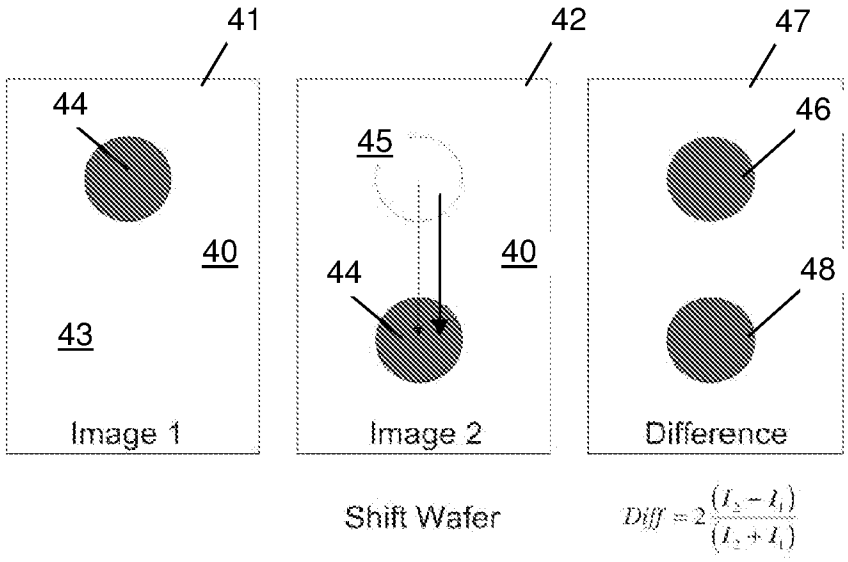

Figure 5

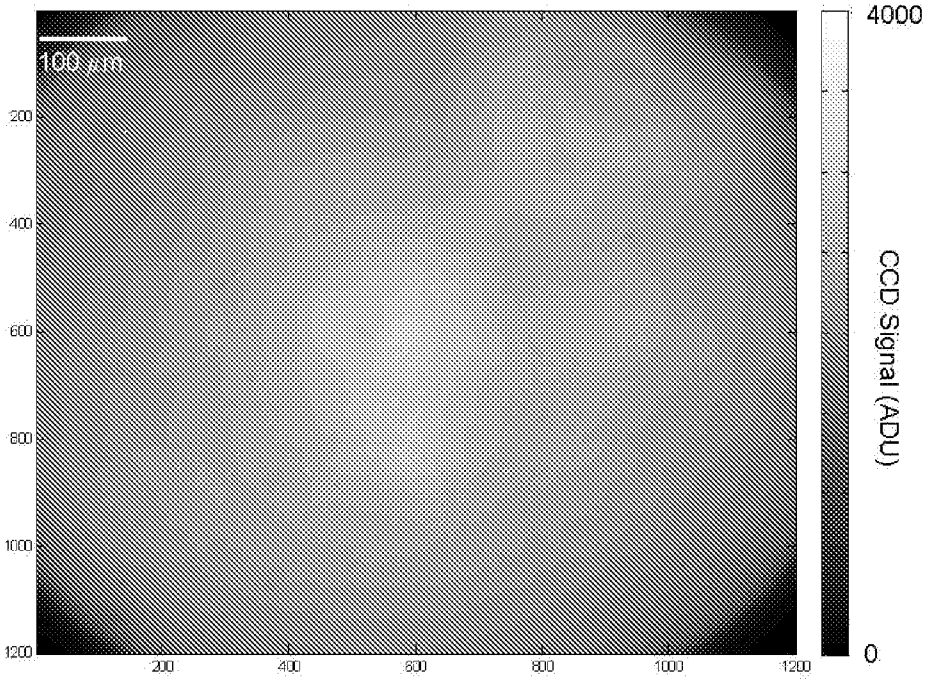

Figure 6A

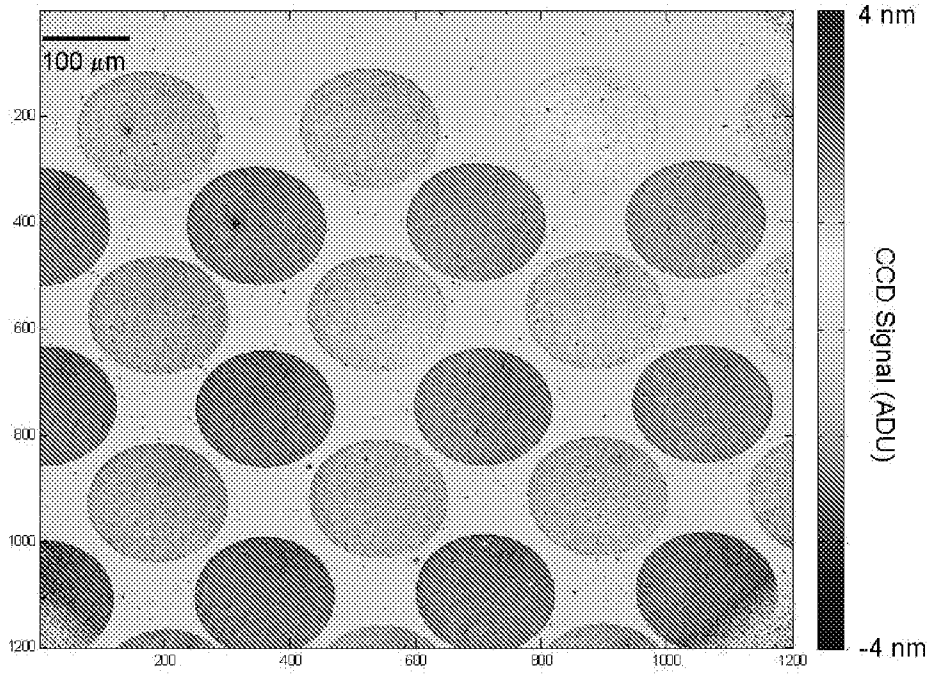

Figure 6B

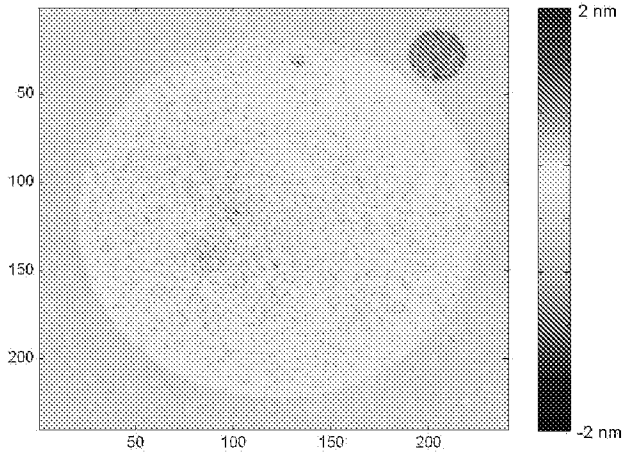

Figure 7A

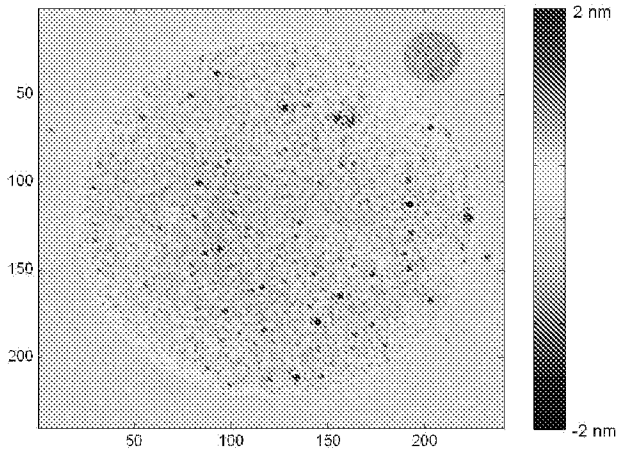

Figure 7B

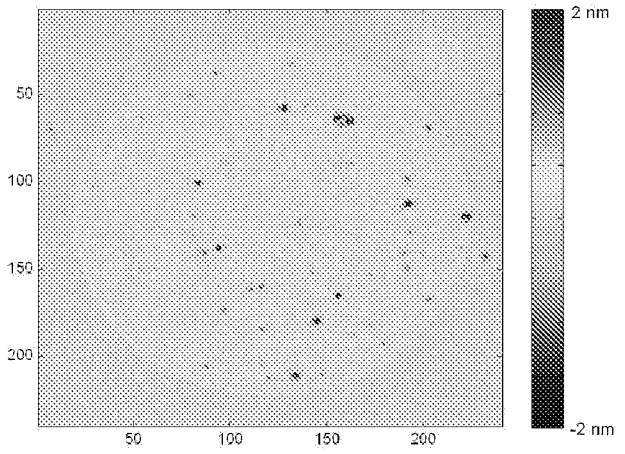

Figure 7C

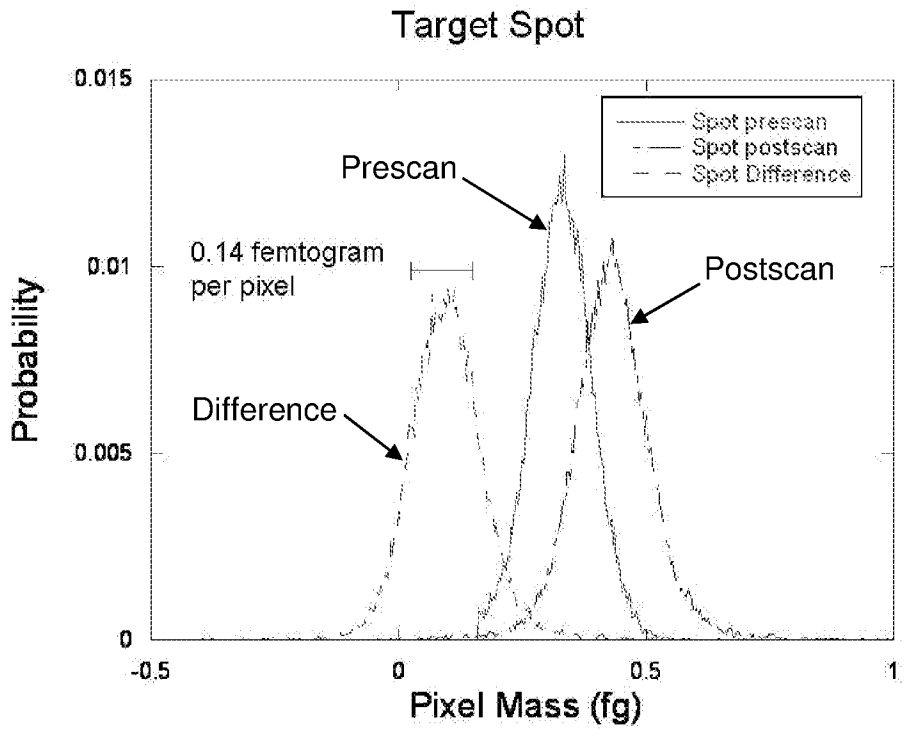

Figure 8A

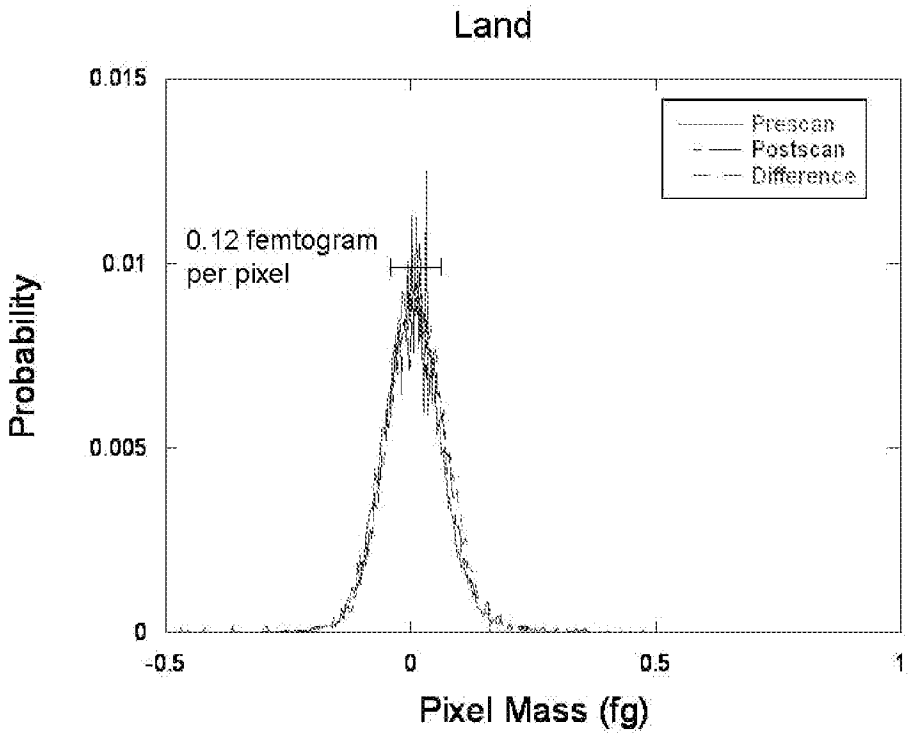

Figure 8B

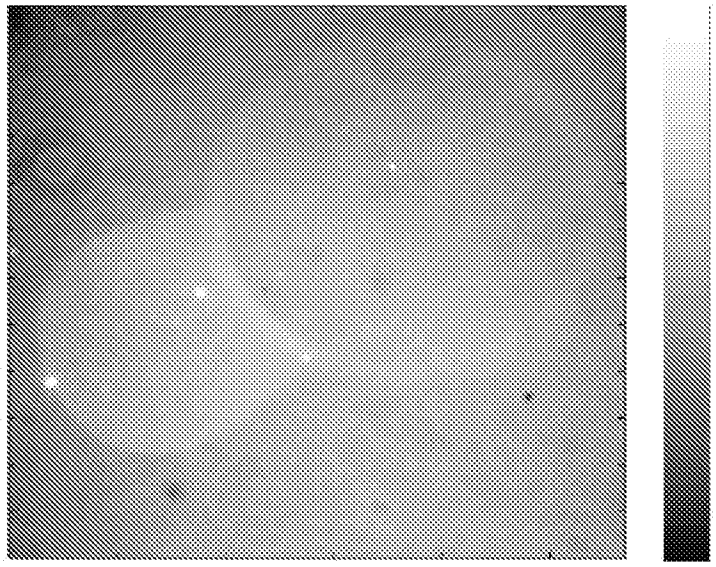

Figure 9A

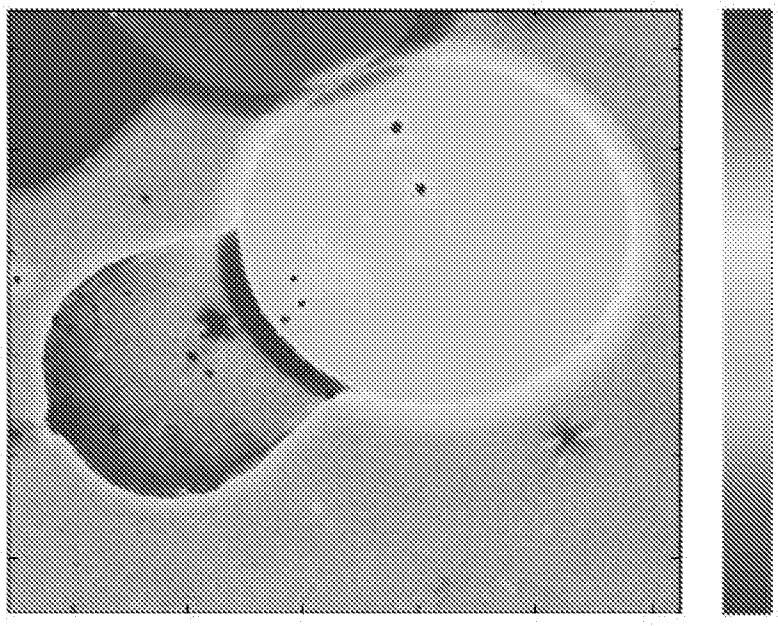

Figure 9B

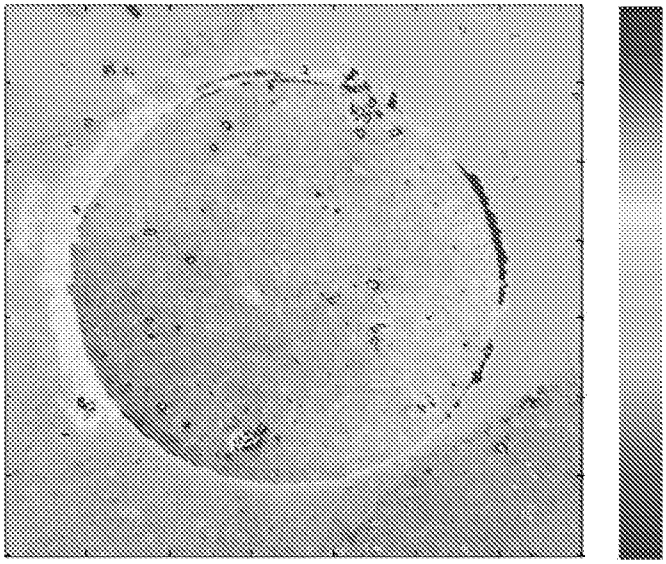

Figure 10

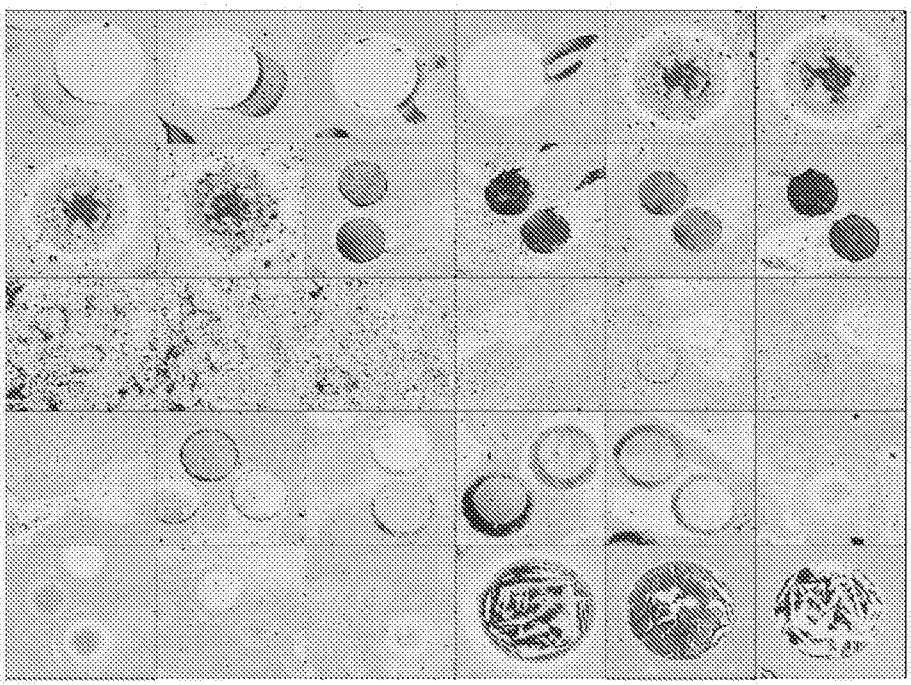

Figure 11

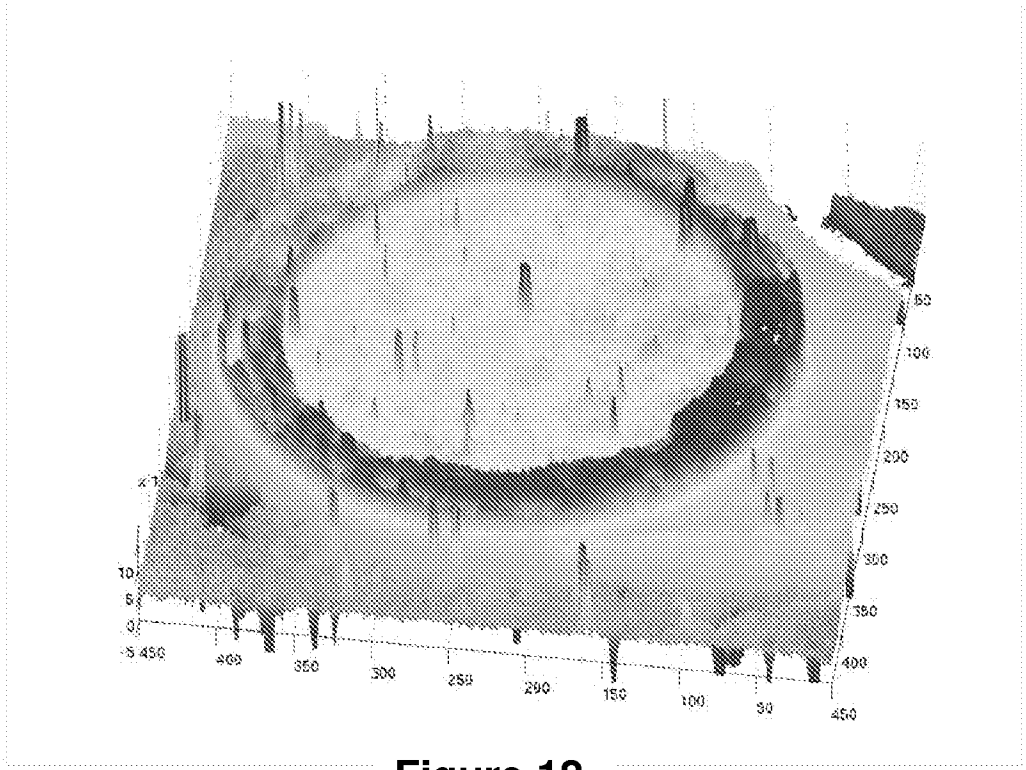

Figure 12

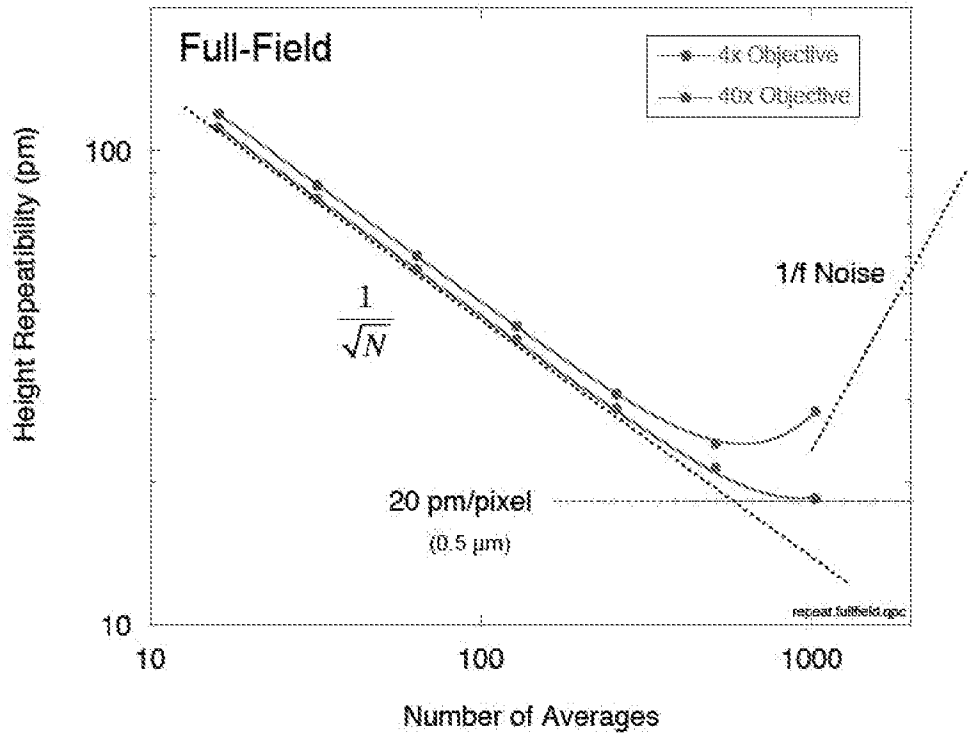

Figure 13

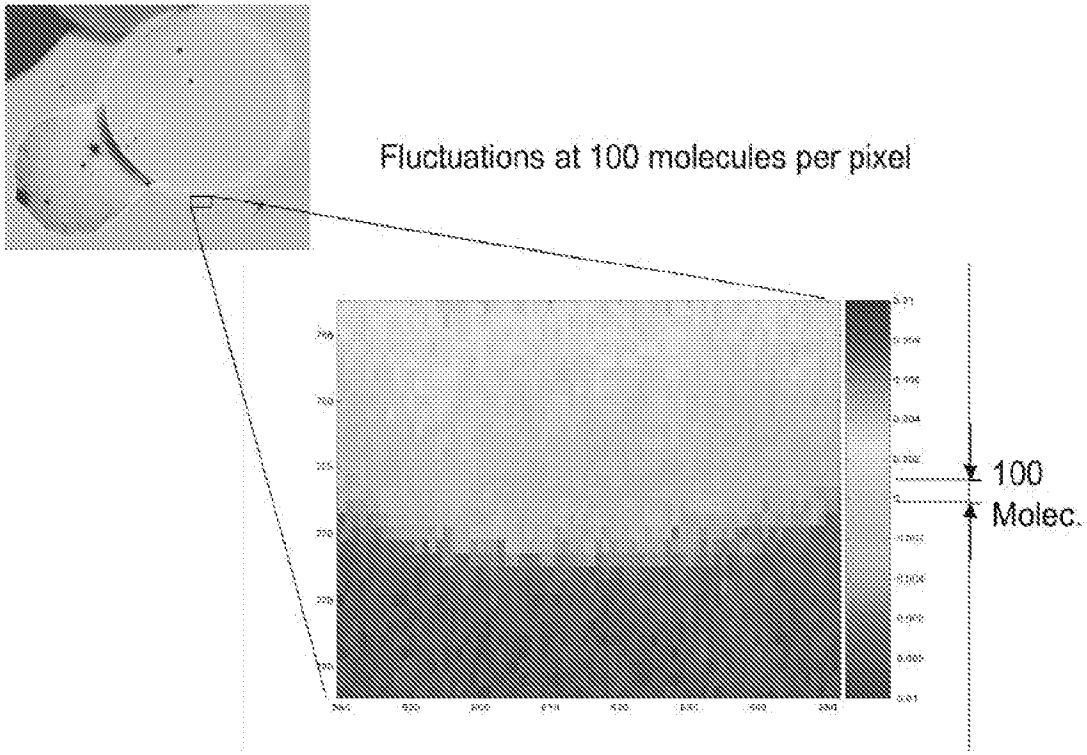

Figure 14

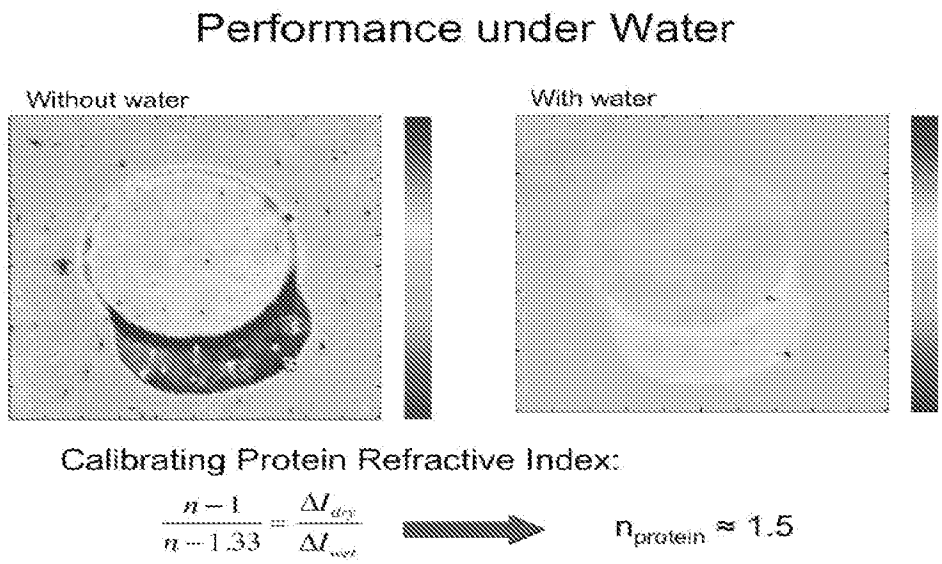

Figure 16

Figure 15

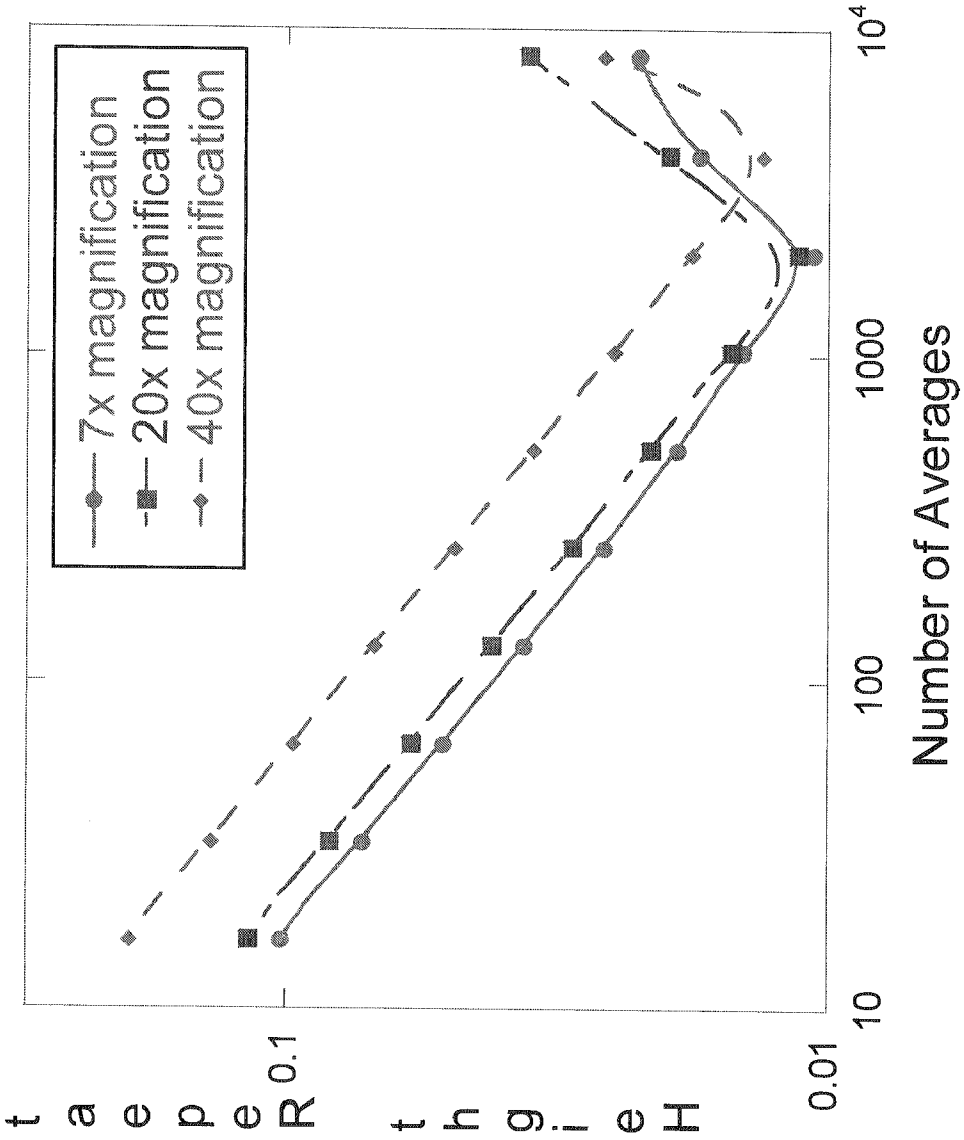
7x magnification
20x magnification
40x magnification
Peak Height
0.1
0.01
10
100
1000
10^4
Number of Averages

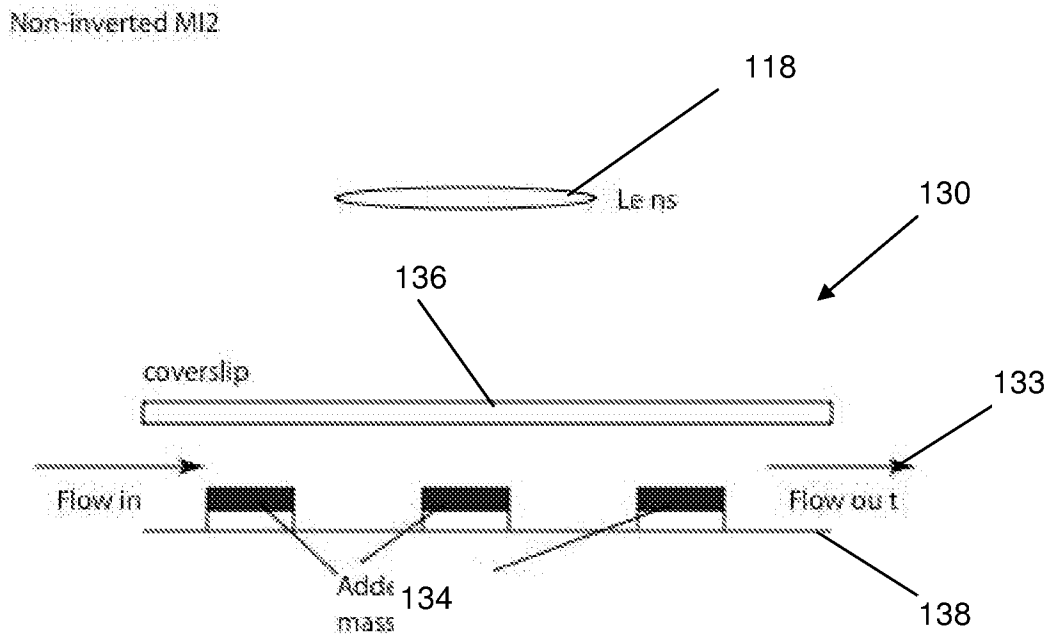

Figure 17

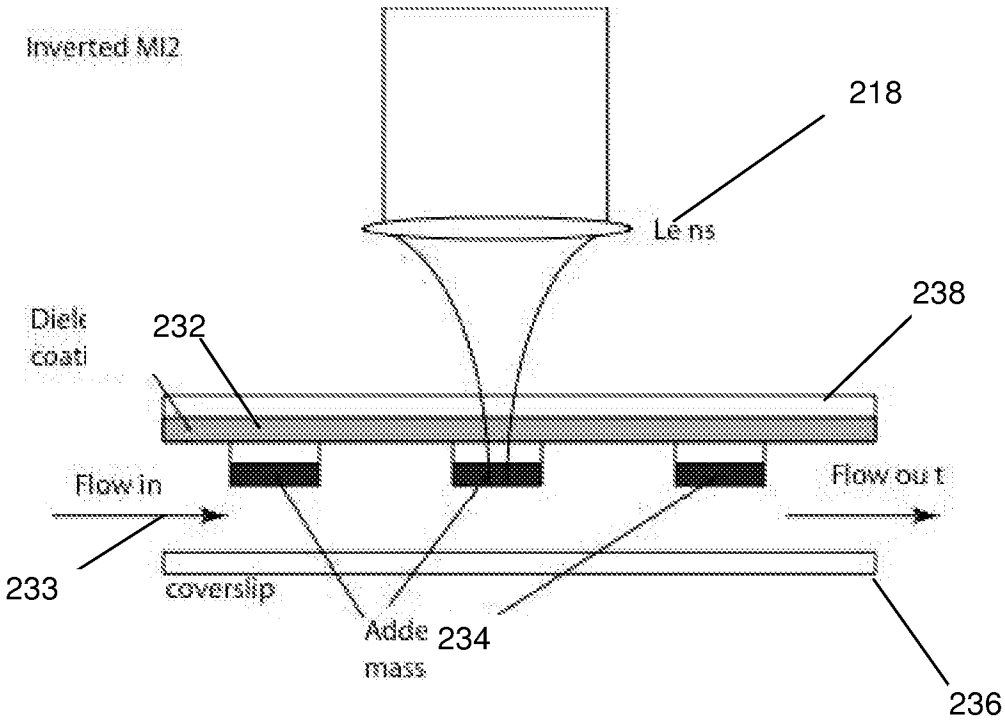

Figure 18

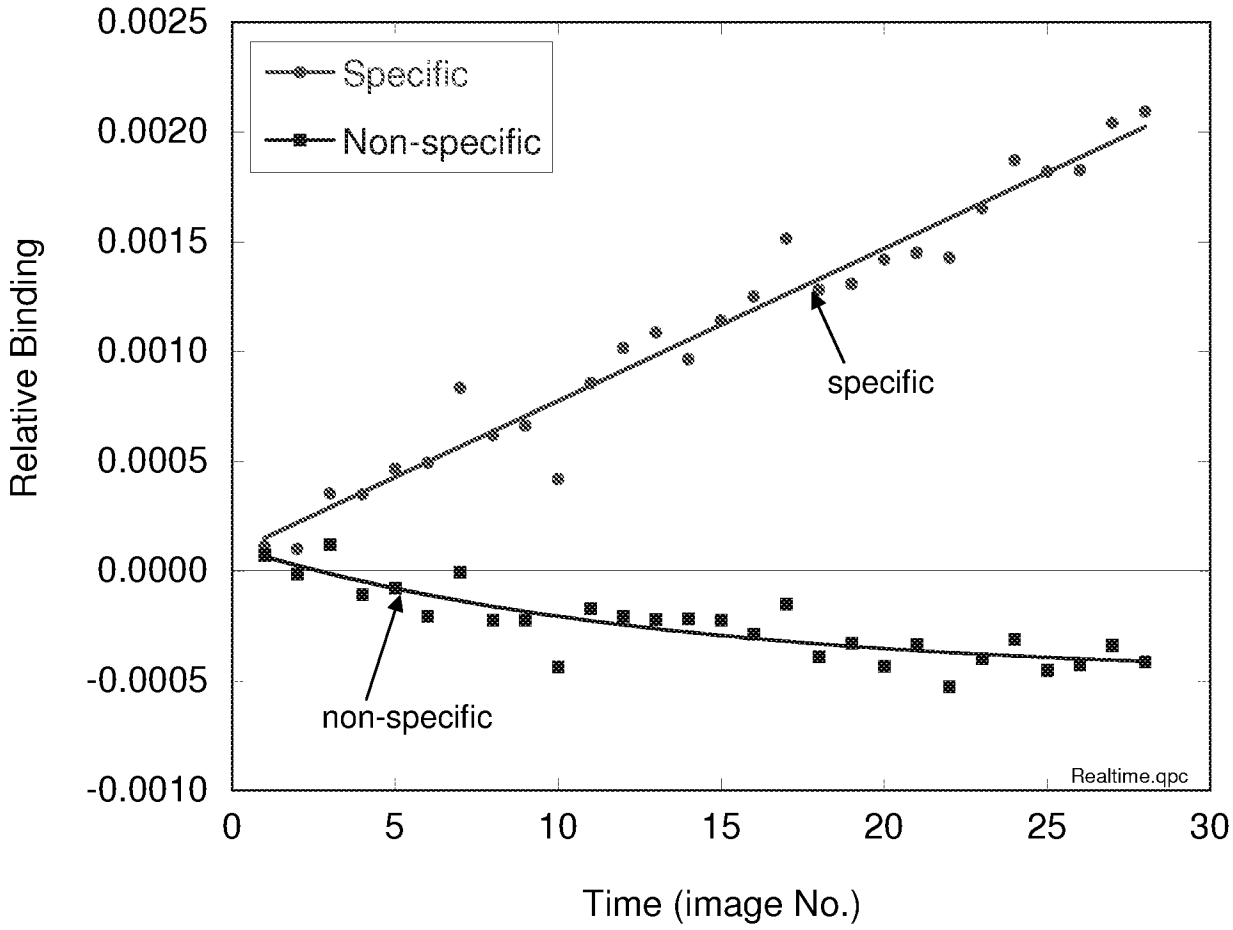
0.0025
0.0020
0.0015
0.0010
0.0005
0.0000
-0.0005
-0.0010
Relative Binding
Specific
Non-specific
specific
non-specific
Realtime.qpc
0
5
10
15
20
25
30
Time (image No.)

Figure 19

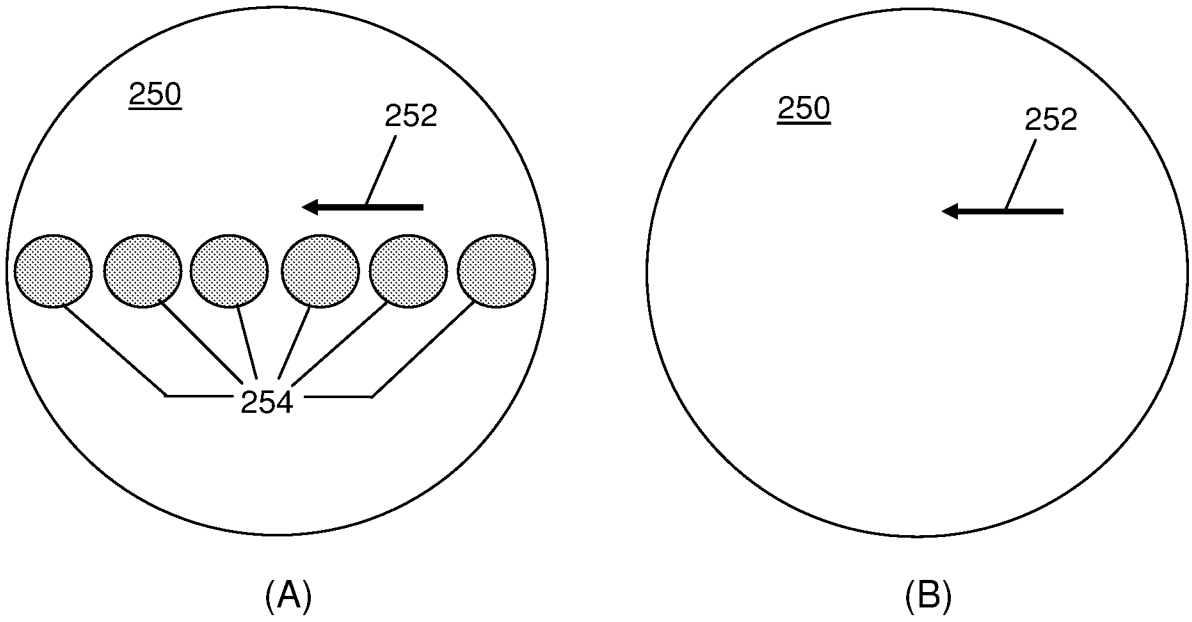

Figure 20

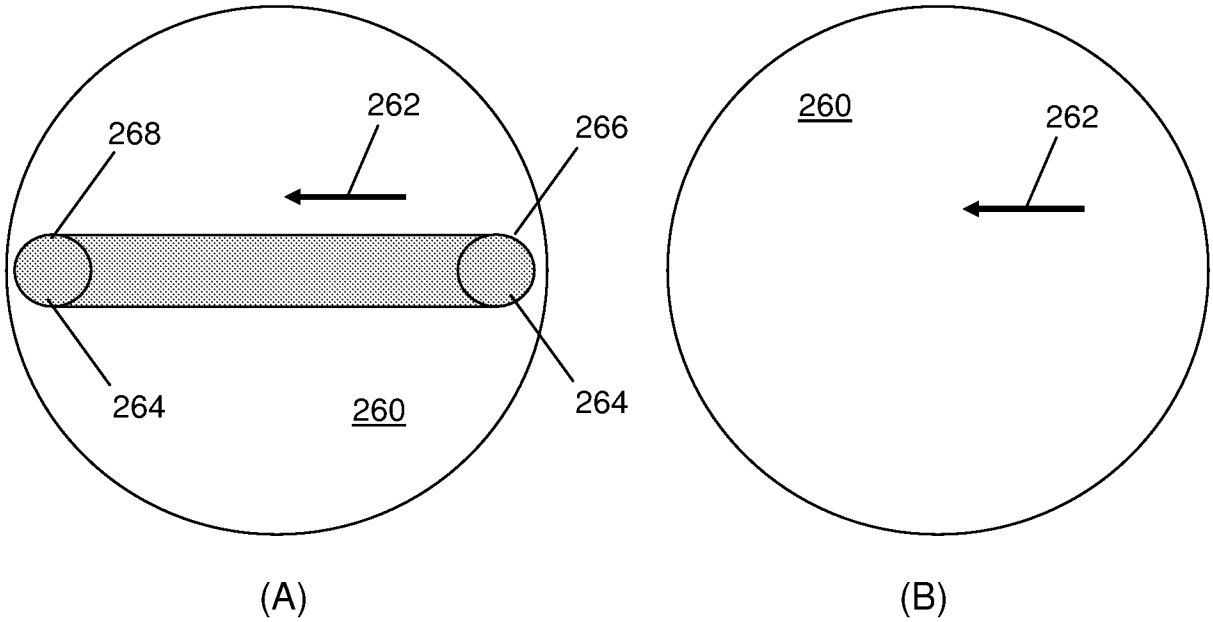

Figure 21

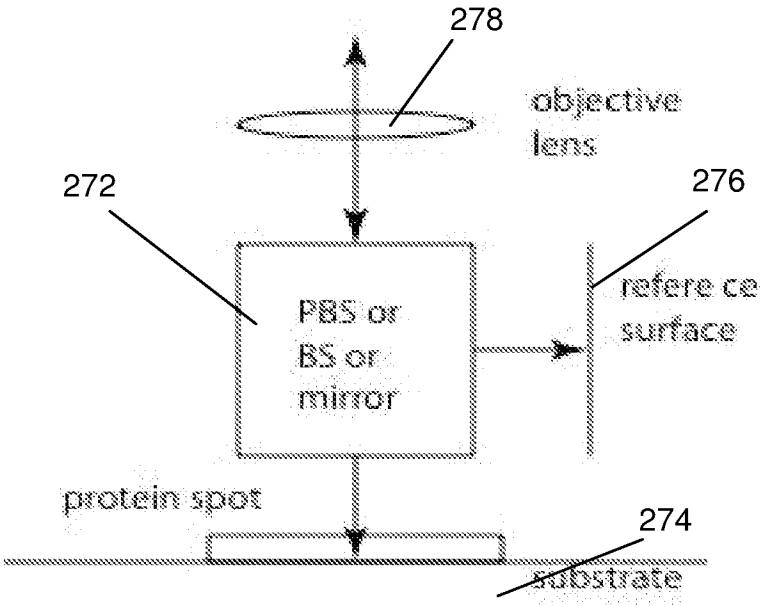

Figure 22

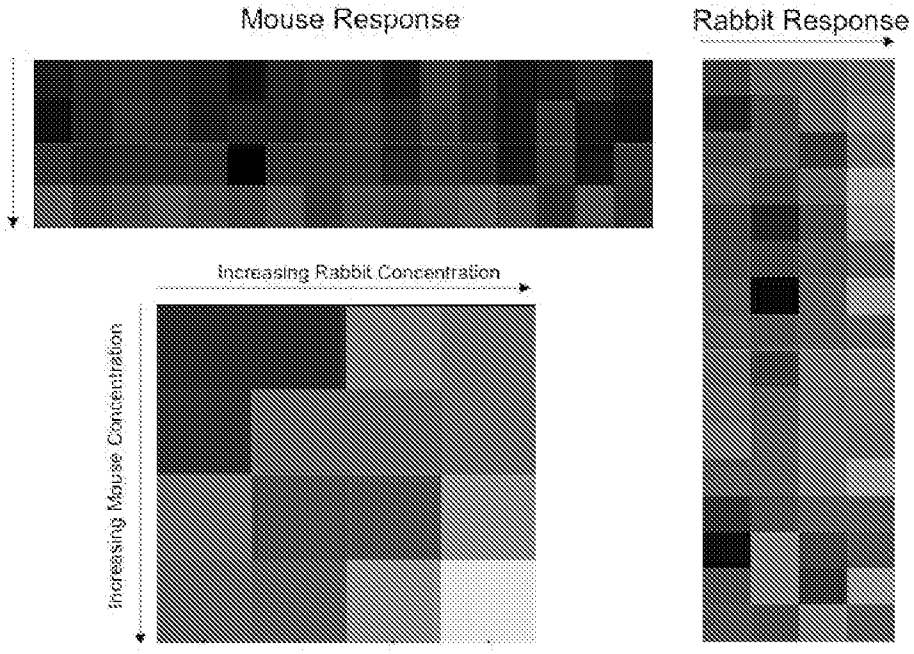

Figure 23

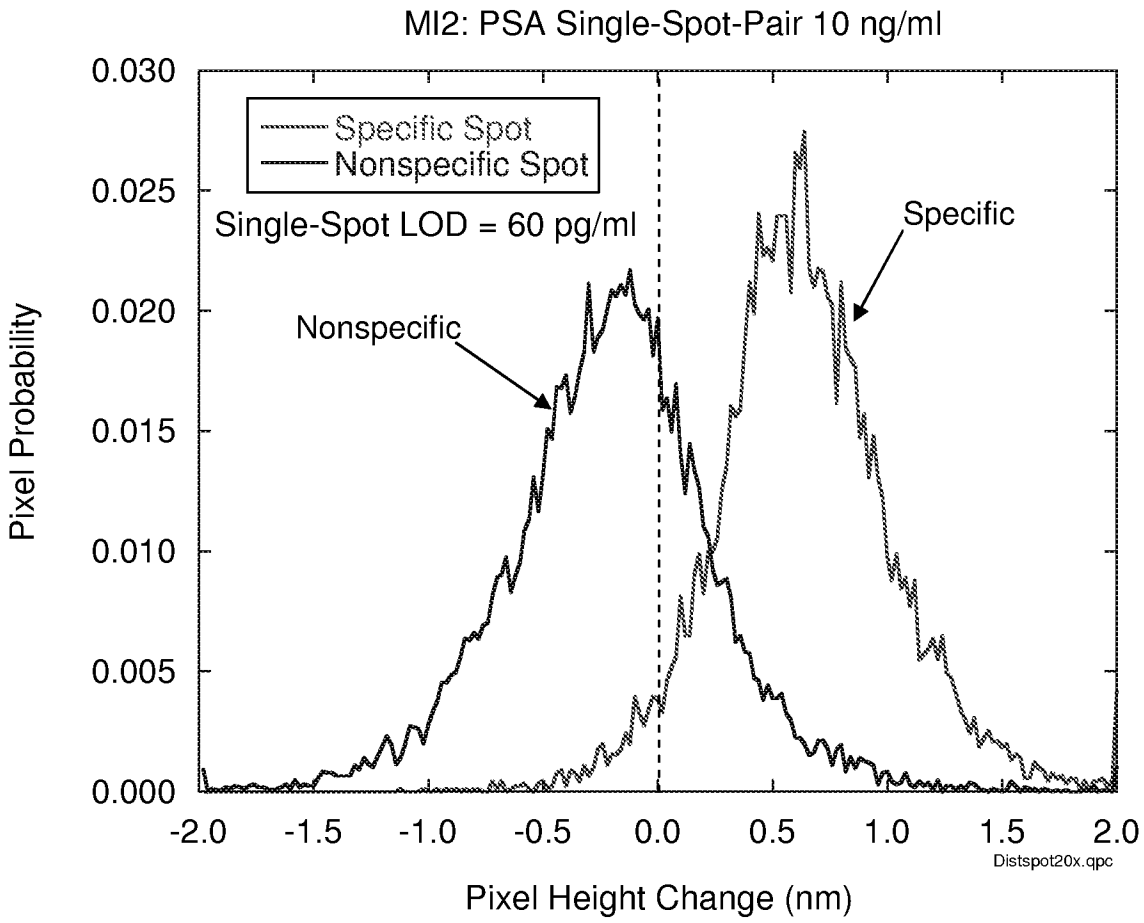
MI2: PSA Single-Spot-Pair 10 ng/ml
Specific Spot
Nonspecific Spot
Single-Spot LOD = 60 pg/ml
Specific
Nonspecific
Pixel Probability
0.030
0.025
0.020
0.015
0.010
0.005
0.000
-2.0
-1.5
-1.0
-0.5
0.0
0.5
1.0
1.5
2.0
Distspot20x.qpc
Pixel Height Change (nm)

Figure 24

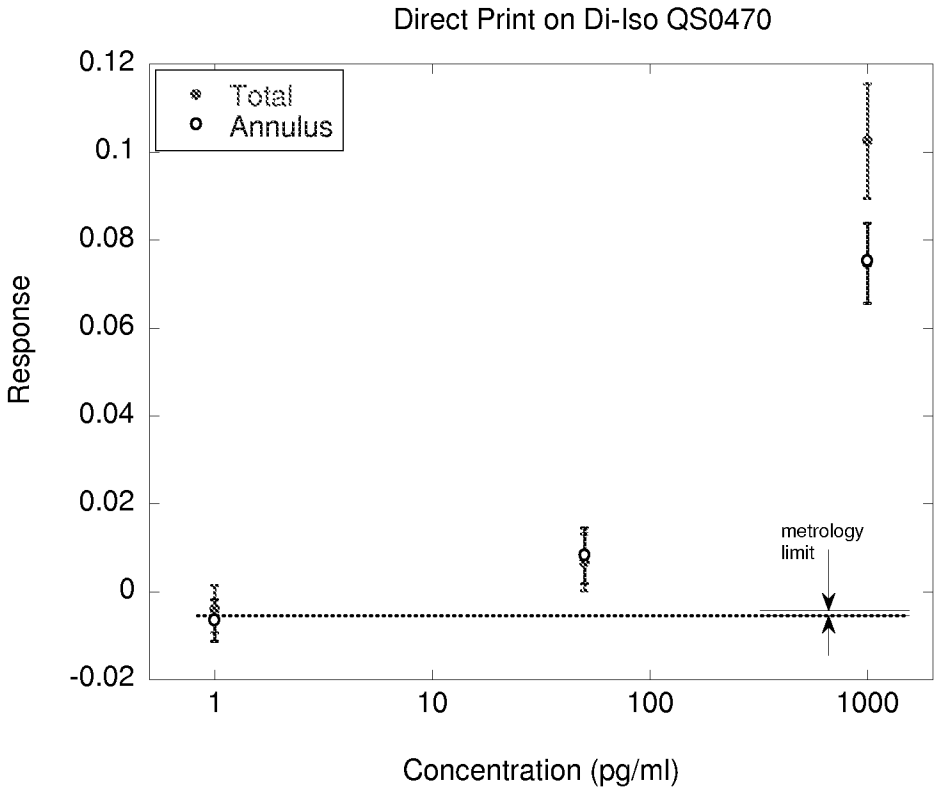

Figure 25

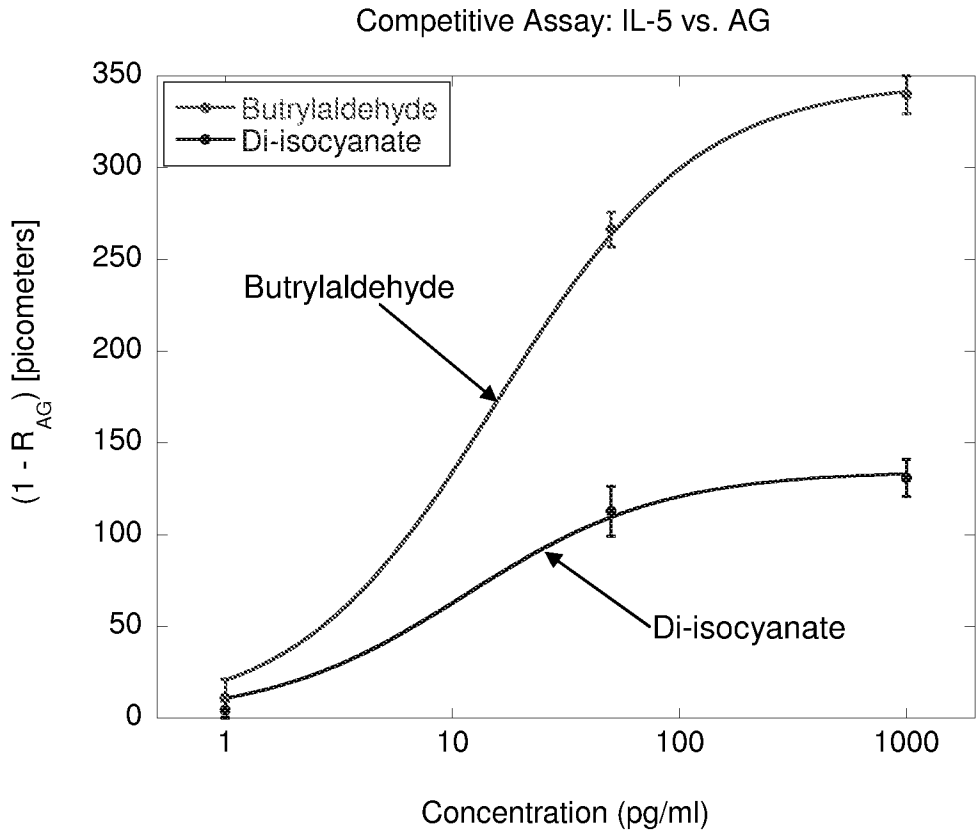

Figure 26

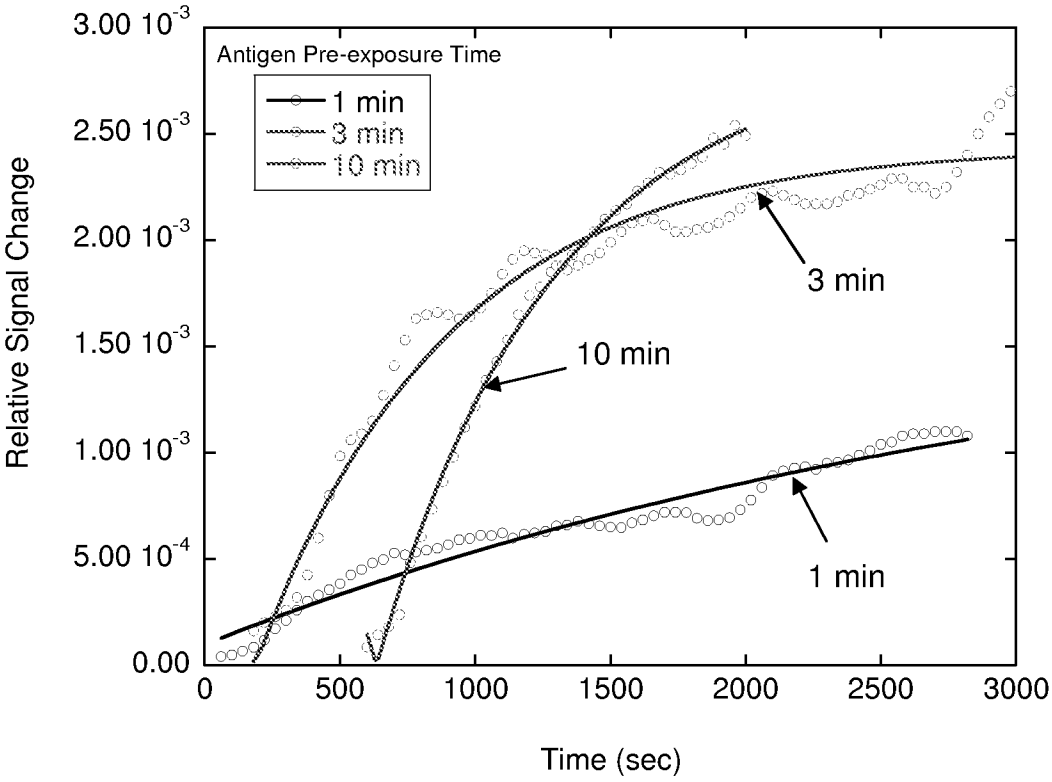

Figure 27A

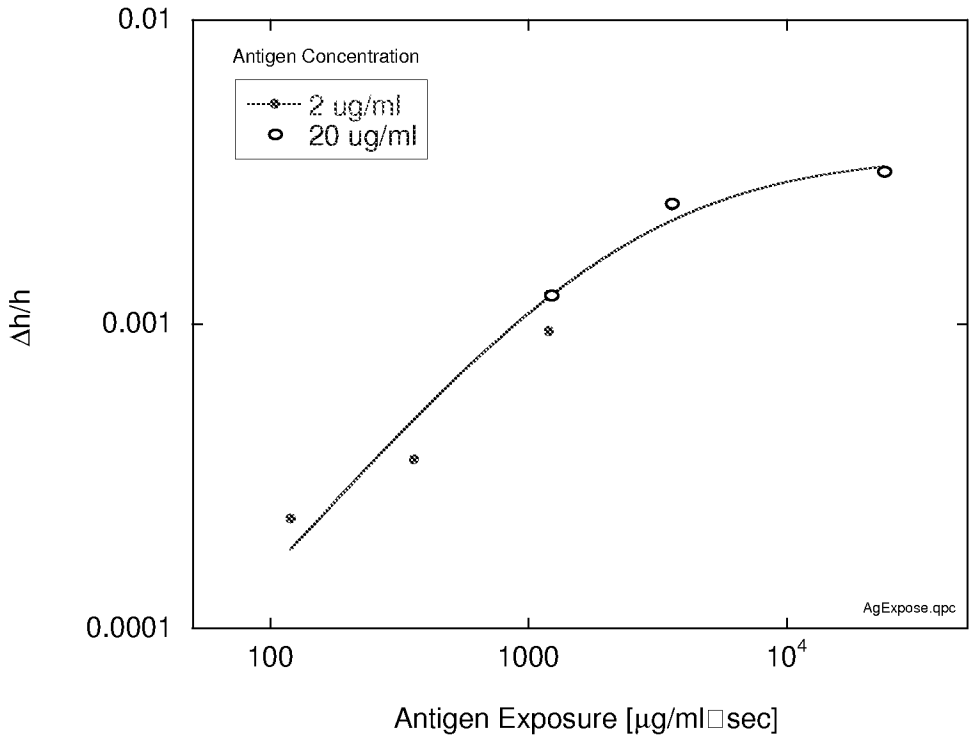

Figure 27B

Figure 28

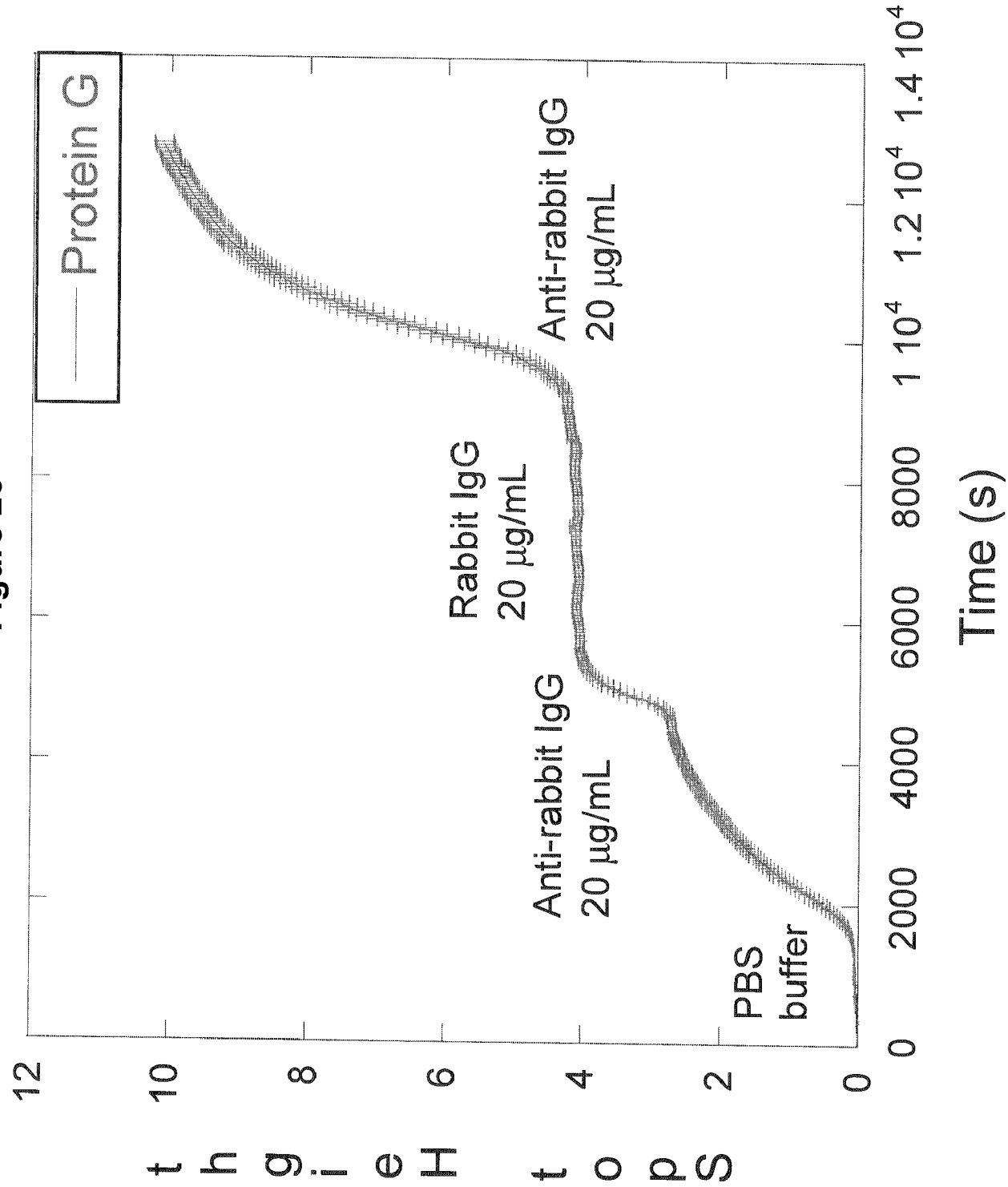
Protein G
Rabbit IgG
20 µg/mL
Anti-rabbit IgG
20 µg/mL
Anti-rabbit IgG
20 µg/mL
PBS
buffer
Shift (nm)
Time (s)
0
2
4
6
8
10
12
0
2000
4000
6000
8000
1 10^4
1.2 10^4
1.4 10^4